

Development of a Flatness Scanner and Simulation for Q_{weak} Wire Chambers

Brian P. Walsh

Advisors: Professor David Armstrong, Doctor Klaus Grimm

*Department of Physics, College of William and Mary,
Williamsburg, VA 23188*

May 8th 2007

Acknowledgements

I would like to thank Professor Armstrong and Doctor Klaus Grimm for all of their time, patience, and kindness that they have so generously given to me.

Abstract

Q_{weak} is an experiment at Jefferson Lab that will precisely measure the weak charge of the proton, Q_w^p , by measuring the parity-violating asymmetry in the elastic scattering of the electron proton interaction. If there is a deviation from the predictions of the Standard Model this will be an indication of new physics. Key to this measurement is the use of vertical drift chambers that are being constructed at William and Mary. These drift chambers will require knowledge of the precise positioning of the wires and the flatness of the wire frames that will hold these wires within the chamber. The aim of this thesis is to develop a flatness scanner for the wire mounts and to simulate the effects of imperfectly placed wires.

Table of Contents

1. Introduction	5
2. The Q_{weak} Experiment	6
2.1 Goals and Set Up of Q_{weak}	6
2.2 The Physics of Q_{weak}	9
3. Drift Chambers	10
3.1 The Tracking System	10
3.2 Drift Chambers	11
3.3 Vertical Drift Chambers	14
4. The Flatness Scanner	15
4.1 Experimental Setup	15
4.2 Data	19
4.3 Conclusion	27
5. GARFIELD Simulations	28
5.1 Introduction to GARFIELD	28
5.2 Garfield Simulations	29
5.3 Garfield Results	34
5.4 Garfield Conclusions	38
A. GARFIELD Input	42
A.1 Cell	42
A.2 Field	57
A.3 XT	50

Chapter 1

Introduction

The first half of this project has been focused on aspects of the construction of a wire chamber, with an emphasis on the development of a laser system to precisely measure the height variation of the wires within elements of the drift chambers. The second half of this work has focused on simulations of wire chambers that have wires that are offset from their nominal positions in order to understand the sensitivity of the apparatus to this feature.

The set of drift chambers that will be constructed are integral parts of the Qweak experiment that will be conducted at Jefferson Lab [3]. This experiment is designed to make the first precise measurement of the weak charge of the proton, $Q_w^p = 1 - 4\sin^2\theta_w$. Integral to this experiment are three components that serve as a tracking system, and which will determine the kinematics of the scattered electrons and measure background contributions of the apparatus. One of these components is a set of vertical drift chambers, which is the responsibility of the William and Mary group.

The key motivation behind this measurement is to further scrutinize the Standard Model and determine the weak charge of the proton which is precisely predicted by the Standard Model. The Standard Model is a theory that was developed in the 1970s to combine the strong, weak, and electromagnetic forces in a way that made them consistent with quantum mechanics and special relativity. However, it is generally felt that this is an incomplete theory. To date, however, all confirmed experiments that have been

performed have agreed with the Standard Model to within three standard deviations of the predicted value.

Chapter 2

The Q_{weak} Experiment

2.1 Goals and Set Up of Q_{weak}

Q_{weak} is designed to make the first precise measurement of the weak charge of the proton at low momentum transfer. This will be done by utilizing the weak force's parity-violation in electron proton elastic scattering. The weak mixing angle, $\sin^2\theta_w$, which is related to the relative effect of the electromagnetic force to the weak force varies with momentum transfer according to Figure 2.1 [3]. This Figure shows the prediction of the Standard Model (SM) along with the results of experiments that have been run so far. The major limitation of these experiments is the error bars, which on all but the measurements conducted at the Z-pole are so large that they provide only limited information. A measurement at low momentum transfer $Q \sim 0.003 \text{ GeV}$ would allow another point to test the Standard Model [4].

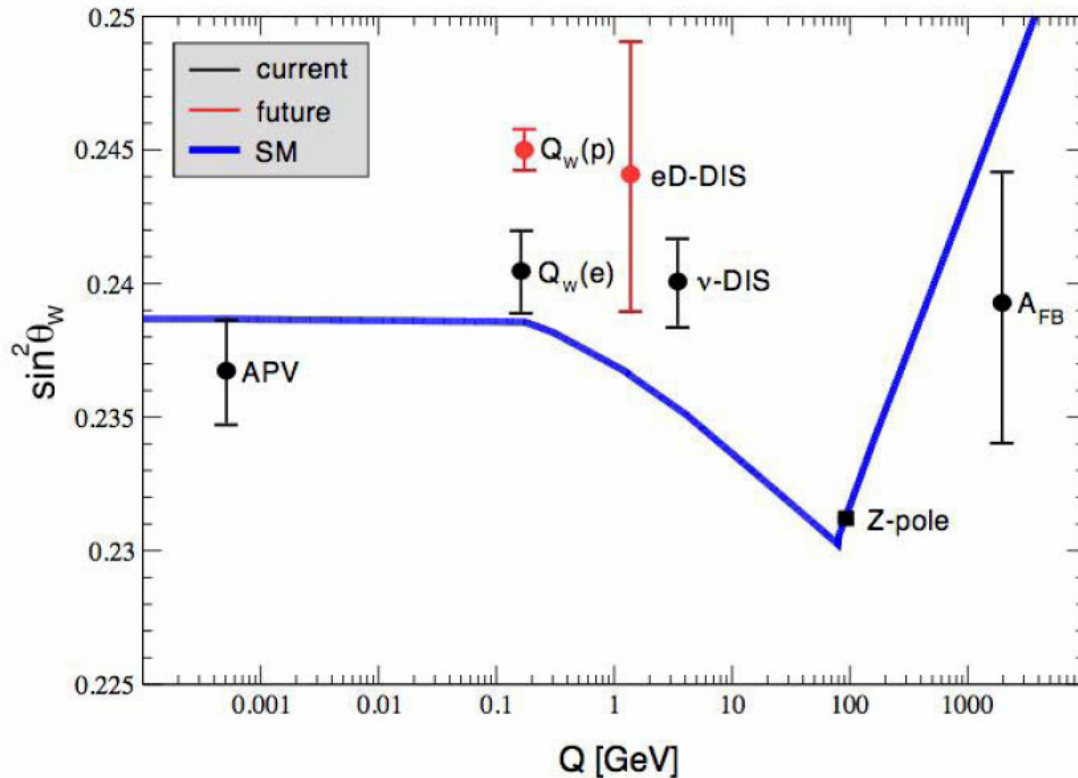


Figure 2.1-Shows the predicted Weak Mixing Angle of the proton along with the results from experiments that have been conducted so far. This Figure also shows two future experiments including Q_{weak} , $Q_w(p)$. These are arbitrarily placed along the y axis but, do show the expected error bars that will be associated with them[3].

This experiment will utilize Jefferson Lab's accelerator to create an 80% polarized 1.2 GeV electron beam that will collide with a 35cm long target of liquid hydrogen. The experiment will then use a series of collimators and a toroidal magnet that will select electrons with a scattering angle of $9^\circ \pm 2^\circ$ [4]. The electrons will then hit one of an array of eight Cerenkov detectors. These detectors will emit bursts of light as the electron passes through. These bursts of light are recorded by photomultiplier tubes that are located on either end of the Cerenkov detectors. These photomultiplier tubes read out to a computer that integrates the voltage for each detector. However, the Cerenkov

detectors do not produce a uniform response due to the conical nature of the optical boom, so it is necessary for a tracking system to be employed. This tracking system will ensure that the Cerenkov detectors are measuring elastically scattered electrons and will determine the electron's Q^2 .

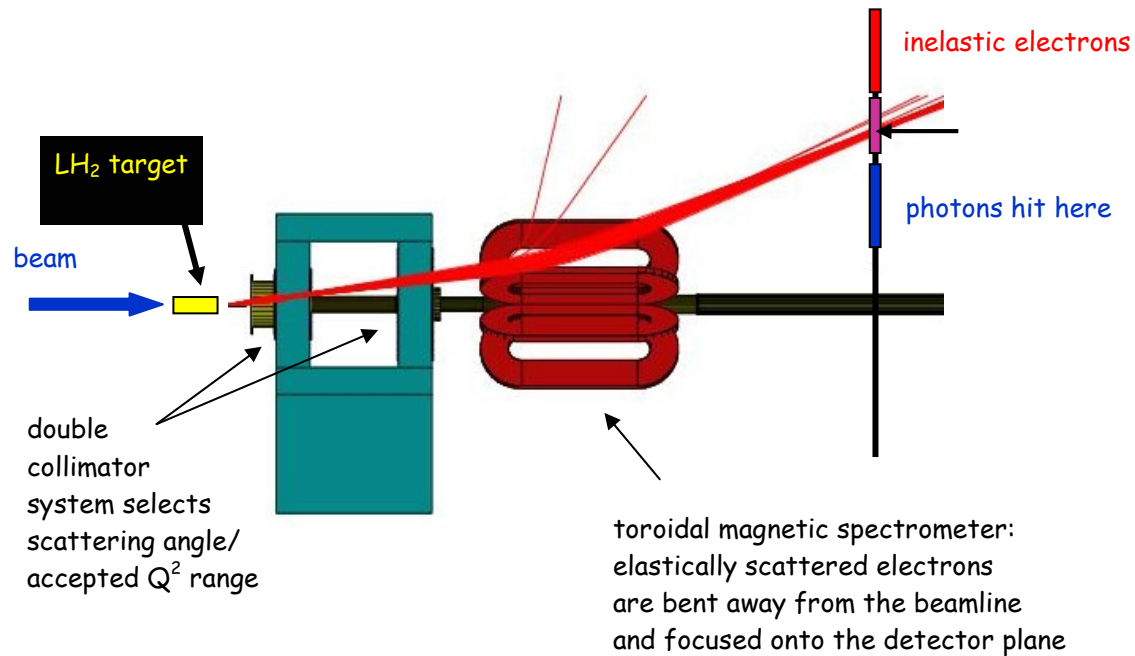


Figure 2.2-Overview of the Q_{weak} apparatus [8].

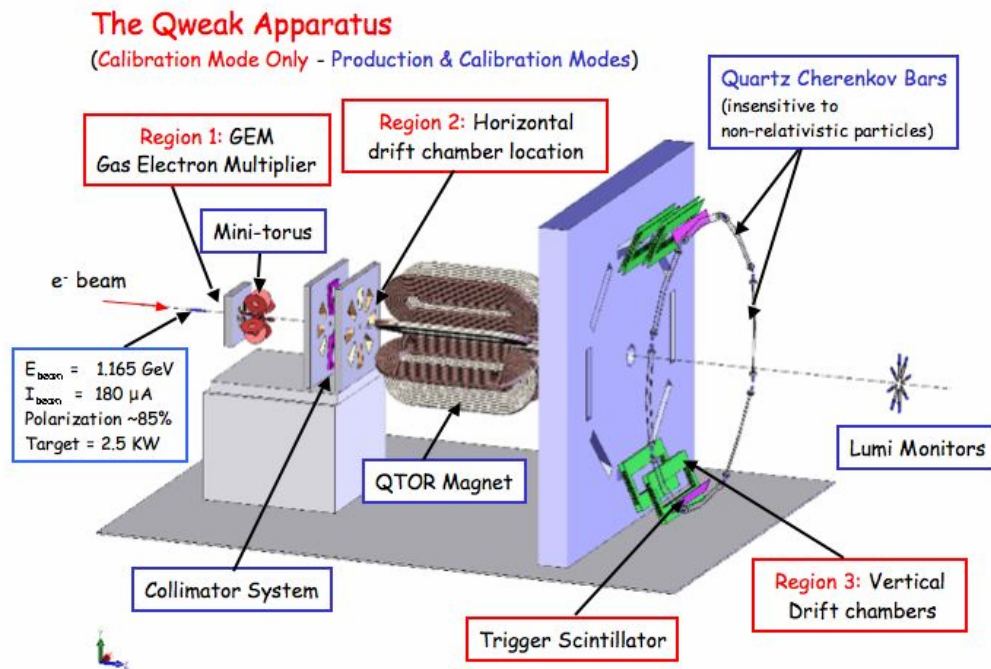


Figure 2.3-Shows the planned experimental set up for Qweak. The regions in red designate apparatus that will assist in the calibration of the experiment [8].

2.2 The Physics of Q_{weak}

The weak force is one of three fundamental forces described by the Standard Model and is the only one that is parity-violating; the effect of the weak force changes with a spatial inversion. The weak force is carried by three particles W^+ , W^- , and Z^0 and none of these particles interact the same with fermion particles. The W^+ particle interacts only with right-handed fermions, particles whose spin is parallel to the electron beam. The W^- boson only interacts with left-handed fermions, particles that have a spin

antiparallel to the electron beam. The Z^0 interacts with both right-handed and left-handed fermions but with unequal magnitudes.

$$M_{LH}^{Z^0} \neq M_{RH}^{Z^0}$$

This asymmetry of the Z^0 interactions, A_{LR} , is defined as the difference in reaction cross sections between left-handed and right-handed polarized electrons divided by the sum of the two cross sections:

$$A_{LR} = \frac{\sigma_+ - \sigma_-}{\sigma_+ + \sigma_-}$$

This is in turn proportional to the weak charge of the proton and the momentum transfer as given below.

$$A_{LR} \propto Q^2 Q_{weak}^P + A_S Q^4$$

The constant, A_S , is related to the strong force's effects. Since the momentum transfer Q^2 will be rather low, 0.03 (GeV)^2 the effects of the strong force will be minimized, resulting in the asymmetry being proportional to the weak charge. From the A_{LR} it is possible to determine the Weinberg Angle for low momentum transfer from the relationship:

$$Q_{weak} = Q_w^P = 1 - 4 \sin^2 \theta_w$$

The Weinberg Angle can then be compared to the predictions of the Standard Model.

Due to the very small difference in the Z^0 interaction with the right-handed fermions and left-handed fermions and the desire for a high experimental precision it is necessary to make on the order of 10^8 measurements. To achieve this goal the electron beam's polarization will be changed randomly by a computer thirty times a second.

Chapter 3

Drift Chambers

3.1 The Tracking System

Crucial to the experiment will be a tracking system that will measure the angles that the electrons enter the Cerenkov detectors, as well as finding the ratio of electrons that elastically scattered to those that did not elastically scatter off the hydrogen target. As Figure 3.1 shows, there is no guarantee that an electron that hits the Cerenkov detectors did not interact with any of the apparatus in the experiment. During the calibration of the experiment the beam intensity will be adjusted so that there is only one Cerenkov “hit” at a time. It should then be possible to recreate the exact track of each electron. The focus of the William and Mary group has been the development and construction of the “Region III” vertical drift chambers for the tracking system.

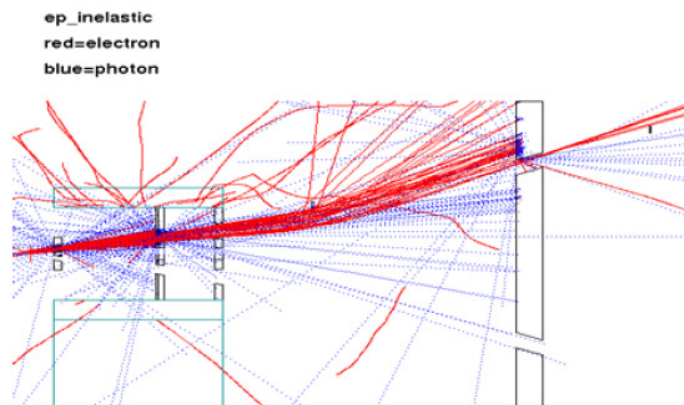


Figure 3.1-Result of a Monte Carlo computer simulation showing many possible electron paths, including those that involve interaction with the apparatus itself. [6]

3.2 Drift Chambers

A drift chamber is a gas-filled cavity that contains a matrix of wires that create an electric field. The purpose of the drift chamber is to measure the location and angle of the primary electron. This is achieved by measuring the drift time of the electrons scattered by the primary electron [5]. This drift time can then be used to determine the drift distance by utilizing a computer simulation program known as GARFIELD. A simple drift chamber contains one wire that is held at virtual ground and is sandwiched between two planes that are held at high voltage as Figure 2.3 shows below. The gas mixture that is used affects the drift time of the electrons and so the Argon ethane mix that has been chosen for Q_{weak} has its own special properties.

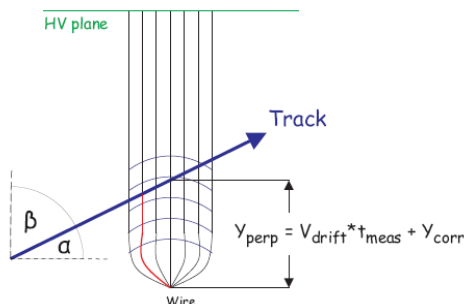


Figure 3.2-Demonstrates a single cell of a Drift Chamber with its associated electric field lines and isochrones. The red line indicates the path of the first electron to hit the wire. The y_{perp} distance is the calculated drift distance from the drift time. [6]

As the high speed electron enters the drift chamber it collides with the gas molecules. This interaction then produces an ionized molecule electron pair. The resulting ionization electrons will then be attracted to the wire which is held at virtual ground. As an electron gets closer to the wire and the strength of the electric field

increases it will gain the ability to create another molecule-ion pair. The two electrons can then produce more electrons as they approach the wire. This increase of the number of electrons approaching the wire is known as the “avalanche effect” and is shown in Figure 3.3 and Figure 3.4 [5]. The time that it takes for the first electron to hit the wire is known as the drift time, and the electron’s associated velocity is known as the drift velocity. The drift velocity is not constant however. The electron starts out slower far from the wire and then its accelerate increasingly becomes nonlinear.

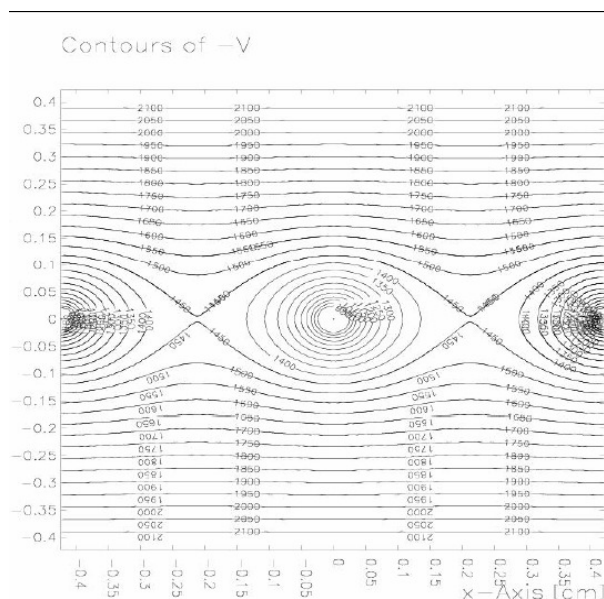


Figure 3.3-Shows GARFIELD simulation of the equipotential lines of the drift chamber. The increasingly dense concentric circles close to the wires demonstrates where the avalanche effect will occur.

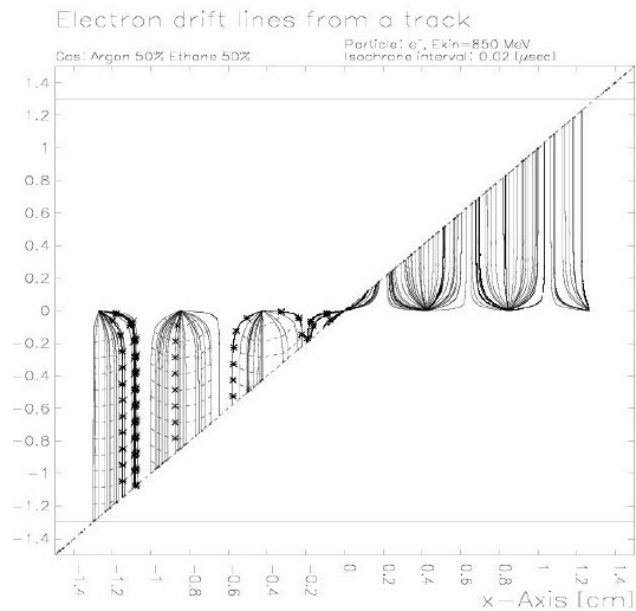


Figure 3.4-Shows a GARGIELD simulation of a track of a single electron entering a drift chamber. The initial electron continues on the path while kicking off other electrons through ionization. These resulting electrons drift toward the wire, following the electric field lines. The high voltage planes are located at $\pm 1.3\text{cm}$ and are charged to -2000V . The wires in comparison are held at virtual ground.

3.3 Vertical Drift Chambers

A vertical drift chamber derives its name from the fact that the shortest path for the incoming particle is in the vertical direction. The Vertical Drift Chambers (VDC) that the William and Mary group has been focusing on will consist of multiple cells arranged in multiple planes as shown in Figure 3.6. The design of the drift chamber is similar to a simple cell, except that now there are multiple wires that run parallel and within a plane at fixed distances from each other. These are then set to virtual ground and sandwiched between two high voltage sheets of foil, and the chamber is pumped with an argon ethane mix. As a high-energy electron scattered from the target transverses the gas in the wire

chamber, it will kick off electrons from the ethane, and these electrons will then be accelerated toward the wires in predetermined paths given by the electric fields.

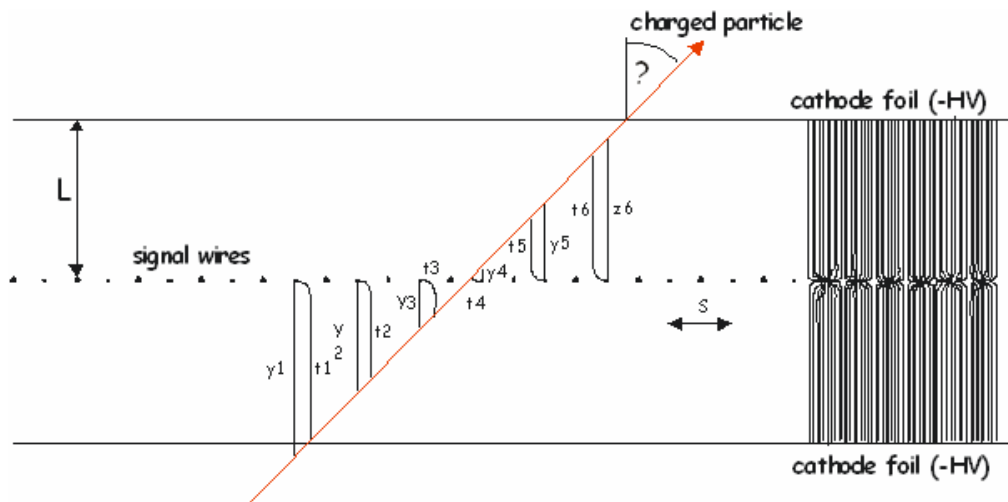


Figure 3.5-Design of the Vertical Drift Chambers that will be used in Q_{weak} . [6]

These drift chambers will provide an initial angle at which the chamber was hit, and a drift time. From the wires that are hit it will be possible to roughly determine the angle at which the electron enters the chamber. From this it was possible to deduce the electron's path through the wire chamber using the GARFIELD simulations. GARFIELD allows a model of the drift chamber to be constructed and, from this it is possible to determine a relationship between the angle, drift time, and perpendicular drift distance. These drift distances will then allow a very accurate trajectory to be constructed. However, for these simulations to be precise the exact placement of the wires must be known, since the electric field within the wire chamber depends on the relation of the wires to one another, the variation of the distance that the wires are placed from one another, and the variance of the height of the wires in relation to one another.

Chapter 4

The Flatness Scanner

The first half of this project has been the development, construction, and implementation of an apparatus that is capable of measuring the height variance of the wire frame to within 20 microns. Because the height of the wires need to be precisely known to simulate the effects of the wire chamber it was necessary to design an apparatus to measure the height of the wires offset from the wire plane.

4.1 Experimental Setup

The experimental set up, as shown in Figure 4.1, consists of a laser and a diode placed at opposite ends of a laser table. The laser photodiode pair is a Sensor Instrument (A-LAS 12/90) that utilizes a Sensor Instrument (AGLR-...-HS) electronic control unit. The laser produced has a rectangular profile and a wavelength of 670nm. The photodiode produced an output voltage that varied according to the amount of laser light that hit it. Gauge blocks were then stacked between the laser and photodiode and measurements were taken to see how height variation affected the output voltage.

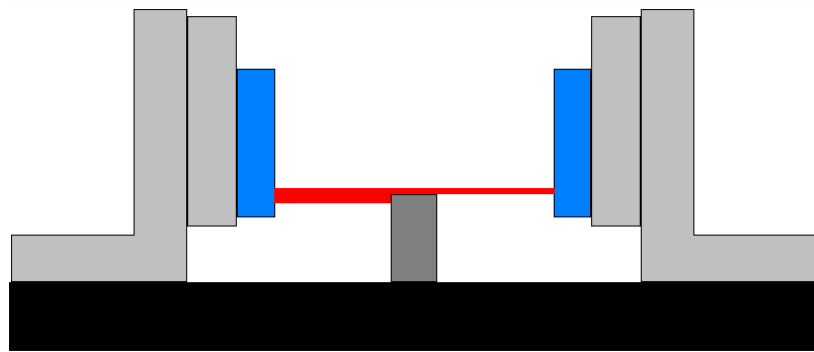


Figure 4.1-Diagram of the laser flatness scanner with the laser on the left.

Figure 4.2 shows the actual set up of the flatness scanner. At either end of the laser are the laser and the photodiode receiver. The electronic control unit is attached to a BK Precision 1760 DC Power Supply unit and a data acquisition board that connects to the computer. The DaqBoard/500 Series was able to read in and store the values as well as calculate the average value of the input. Before each data run the laser would be manipulated to attempt to make the laser beam completely parallel to the laser table. This was done by placing the same set of blocks in front of the laser and the diode and then aligning the laser so that the output voltages were the same.

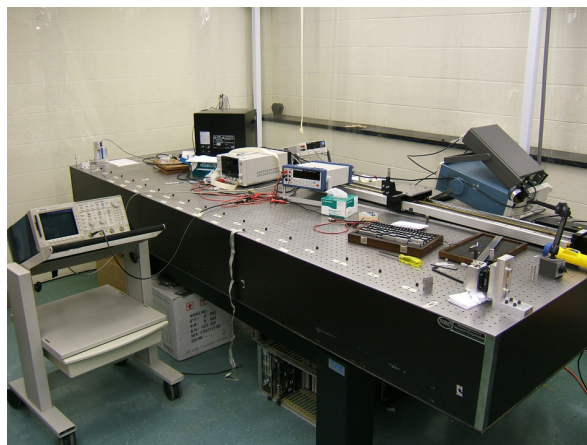


Figure 4.2-Photograph of the laser flatness scanner set up on the laser table.

A problem that was encountered early in the experiment was the limited degrees of freedom with which to align the laser. The initial design only allowed for translation of the laser in the vertical direction. The main failure in this was adjusting the angle of the laser relative to the table. Since the laser was not built to be perfectly perpendicular to its housing and the table itself is not flat, it was necessary to change the angle before every measurement. Also the first design did not allow for adjustment in the horizontal direction. Figure 4.3 shows the ultimate design of the laser mount. It was possible to manipulate the laser precisely in both the vertical and horizontal directions as well as its tilt.

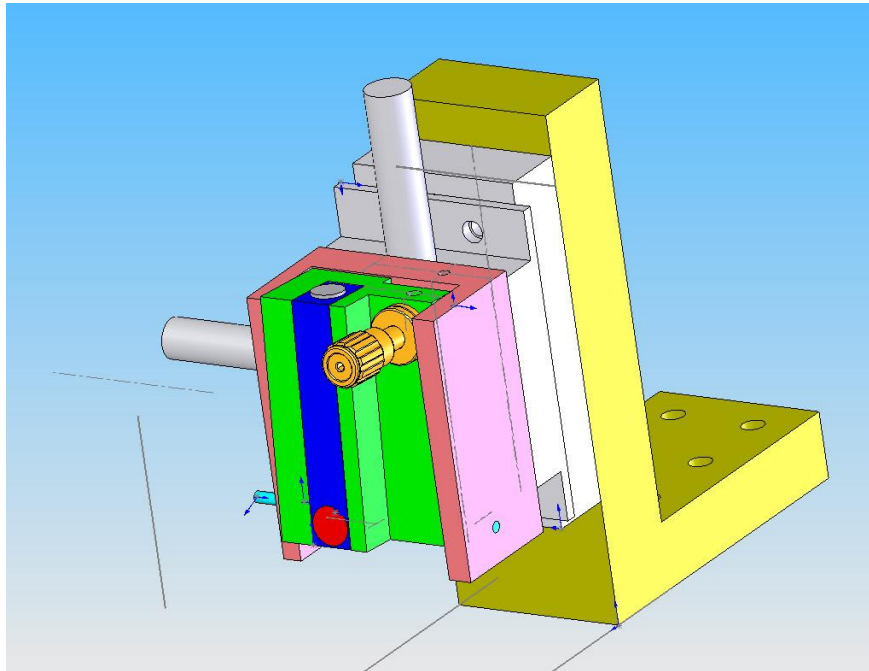


Figure 4.3-Shows the SolidWorks CAD model of the laser mount.

After the laser and photodiode were aligned parallel to the table to the best of the lab's ability, precision gauge blocks were then stacked at various locations on the table. The blocks were then incremented in stages so that the height grew .001" per interval after being cleaned with a Kimwipe to remove any dirt or oil that could block extra laser light. This process started with the blocks not obscuring any light to obscuring all of the laser's profile.

4.2 Data

The first data sets were taken on a granite table that has a guaranteed flatness of $\pm 0.27\mu\text{m}$. Figure 4.4 shows the first set of data. Each data set contains three distinct sets of regions. The first set is the flat ends on either extreme of the graph where the slope approaches zero. This merely indicates the maximum and minimum output of the system. The second distinct region is the linear region which occurs in the center of the graph. This region represents the target area for data collection since it is here that the slope or sensitivity is most constant. The third key region is the transitions between zero slopes and the main linear region. These transition regions are caused by an imperfect rectangular beam profile.

The slope maintains a linear relationship within $\pm 2.5\text{mm}$ of that height at which the gauge block approximately 50% of the laser's profile. In Figure 4.5 just the linear region has been selected and a linear fit applied. The calculated slope for this data set is - 3.26[mV/ μm].

Figure 4.6 shows the residuals of multiple measurements on the granite table when the laser and photodiode were about 8 inches apart as well as one measurement on the laser table with the laser and photodiode 30" apart. These measurements were taken over the course of about an hour and at different times of the day. Given the correlation of the residuals between the granite table and the laser table it seems to indicate either a major flaw with the gauge blocks, or a non-uniform sensitivity of the photodiode or a non-uniform intensity output within laser profile. After measuring the gauge blocks and confirming that they were precise down to 5 microns, it was determined that they were not the cause of the error. From this it seems to indicate that the only cause can be a non uniformity in the laser output or photodiode efficiency.

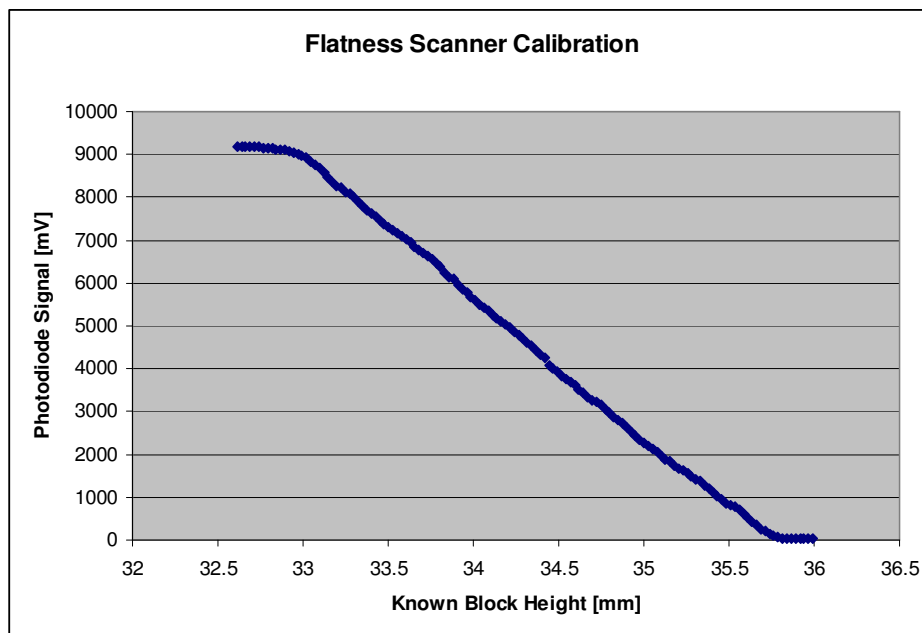


Figure 4.4-First data set of the laser flatness scanner on the granite table.

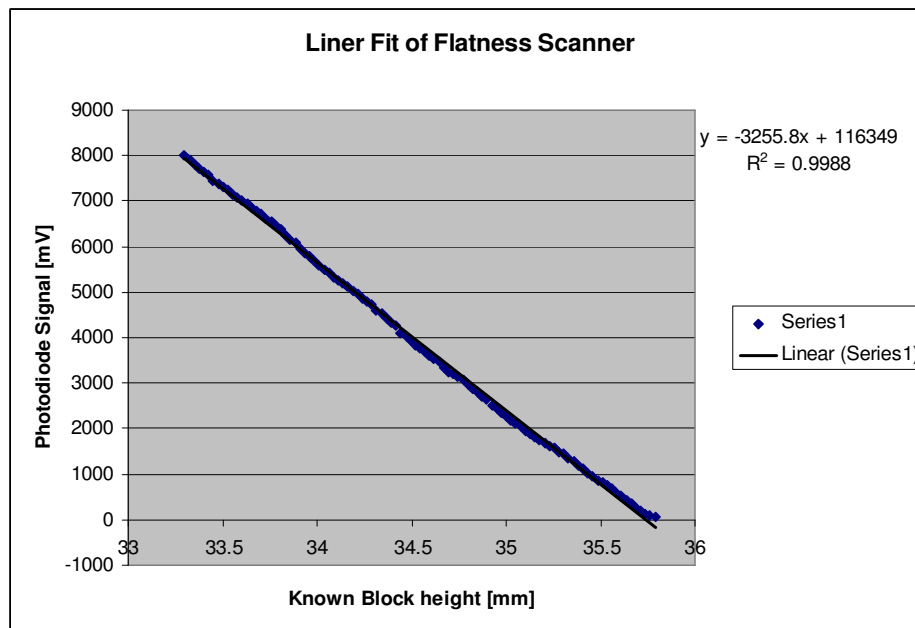


Figure 4.5-Linear region only of the photodiode output.

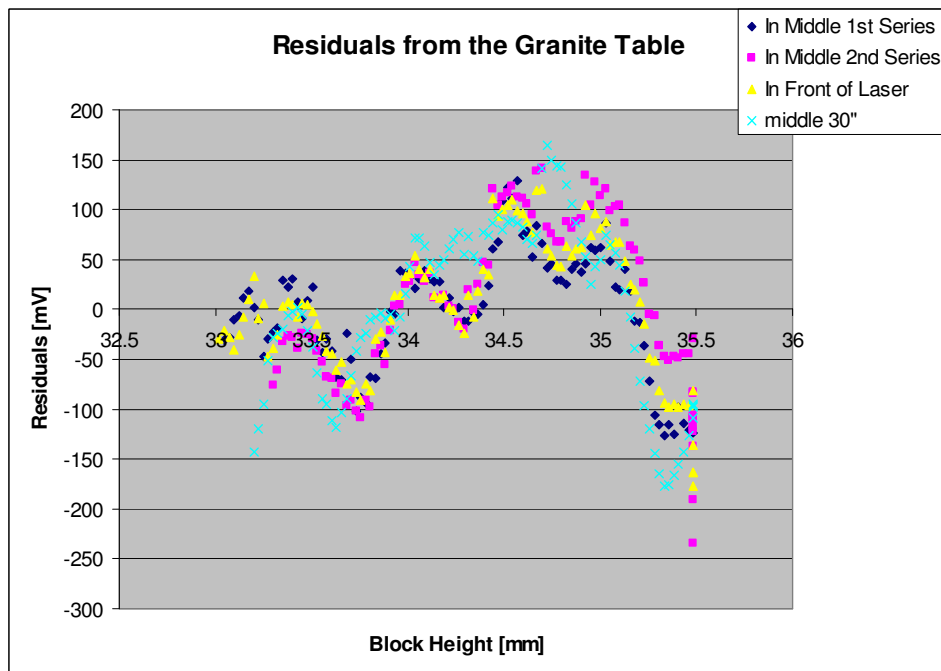


Figure 4.6-Residuals from the granite and laser tables.

In response to these residuals, a closer examination of the laser photodiode pair was made. Figure 4.7 shows the output of the photodiode as the laser was placed

approximately 5 inches away on the granite table. The laser was aligned in the horizontal axis and then placed just above the top of the opening for the photodiode. The laser was then moved in 0.25mm increments until a maximum voltage was obtained. The data was then examined and the linear region taken. This was then fitted with a line and the residuals, that is the difference between the actual measurements and the linear fit, were plotted, Figure 4.8. These high residuals which seem to match the ranges found in the residuals in Figure 4.6 help to confirm that the laser-photodiode pair is the cause of the errors.

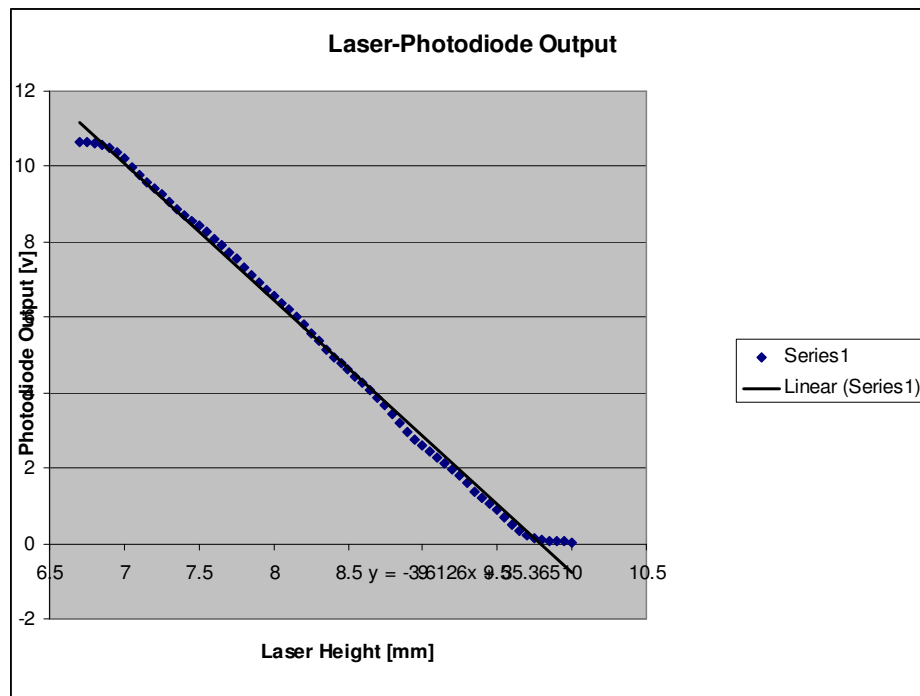


Figure 4.7 Output of the Photodiode in relation to the laser alignment.

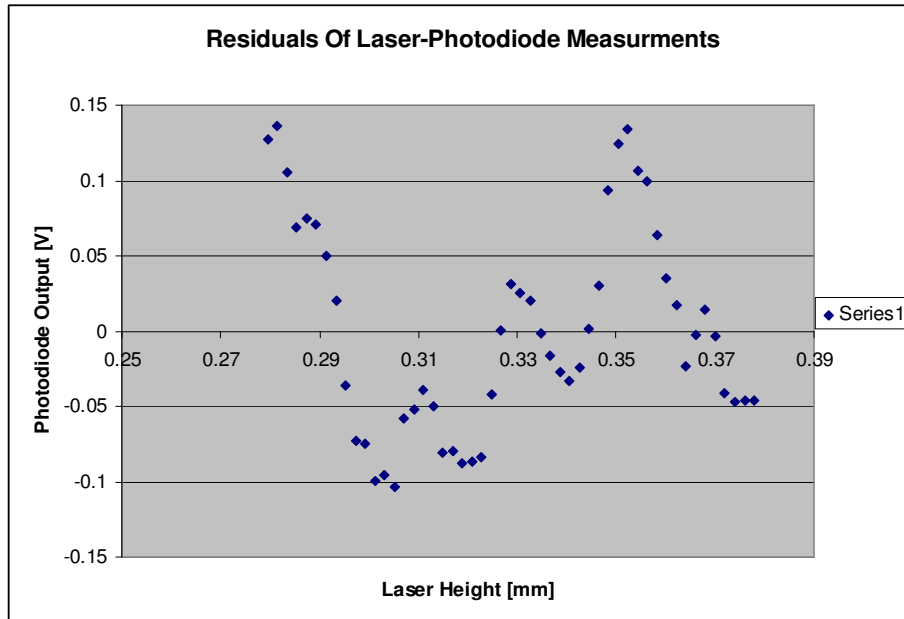


Figure 4.8 Residuals from the Laser Photodiode Height Measurements.

The properties of the laser photodiode at full distance on the laser table were then observed. It was found that the slope varied according to the distance between the laser and diode. The placement of the gauge blocks also affected the slope; however, this seems to be due to problems with making the laser beam parallel. The slope varies with distance between the photodiode and laser because as Figure 4.9 shows the maximum output of a fully aligned arrangement decreases with distance. As a result there is less of a voltage drop over the same amount of gauge block height change. The gauge block placement affects the slope since the laser beam is never completely parallel and so will cut off different parts of the lasers profile. Since the beam will be at an angle the effects of the gauge blocks will be exaggerated, and these effects will increase with distance between the laser and photodiode.

In order to examine this change in slope more closely, the flatness scanner was transferred onto the laser table. There the laser and photodiode were placed at a distance

of approximately 104 inches. However, this created some problems with recording the photodiode output. The signal was very unstable and at the maximum distance of the table, ~104 inches, the signal on the multimeter became completely unreadable. An oscilloscope with an average function was then employed but this still resulted in poor precision. Eventually the DaqBoard was employed and yielded reproducible data. Table 4.1 gives the data for 20 measurements of an unchanged configuration of the flatness scanner. From this data a standard deviation of 3.4mV was calculated which indicates that the measurements that the DaqBoard provides are very reproducible, and should not affect the measurements much more than a micron.

Trial	Photodiode Output V
1	3.976692
2	3.977078
3	3.978328
4	3.977799
5	3.977911
6	3.97815
7	3.978106
8	3.979779
9	3.97839
10	3.972954
11	3.972786
12	3.972639
13	3.971653
14	3.971266
15	3.972175
16	3.971668
17	3.970054
18	3.970286
19	3.969726

Table 4.1-Shows the output of the DaqBoard for 19 measurements taken over the course of an hour.

The relationship between the laser diode distance and the maximum output was then examined. Figure 4.9 shows the relationship between the distance of the laser-photodiode pair to output of the photodiode. This graph depicts two relationships. One is

found with the first four measurements. These are related because at these distances the laser beam can still fit completely into the opening slot for the photodiode. After this distance the dispersion of the laser beam is so great that laser light is lost. Figure 4.10 shows the residuals for the first part of the graph and indicates a very good fit for a second degree polynomial. Figure 4.11 shows the residuals from the second section of the graph and suggest that there is another factor coming into to play at larger distances; this is probably a failure to make the laser beam parallel to the laser table and effects of dispersion.

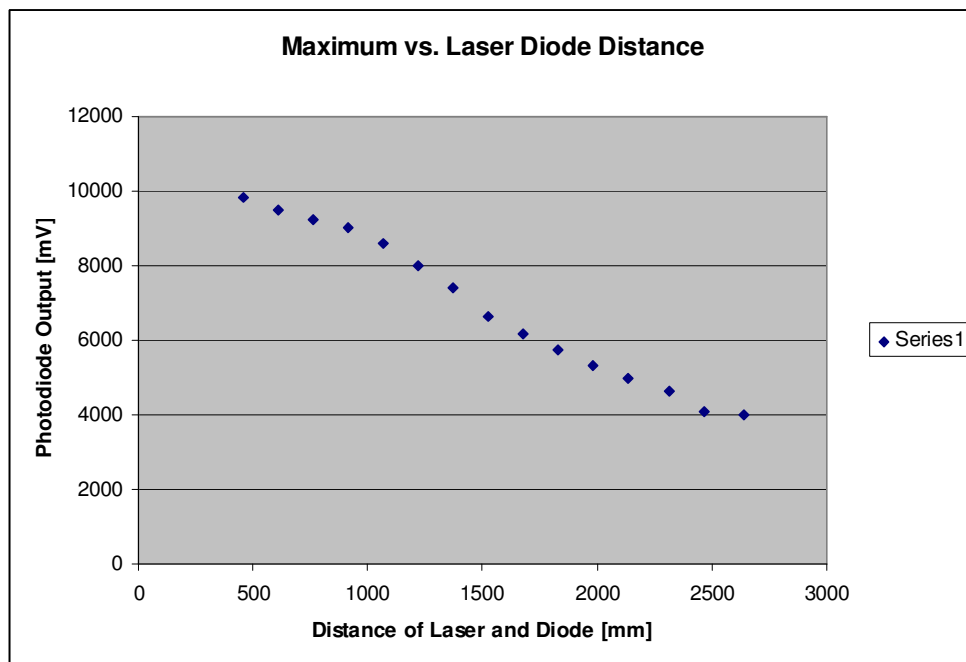


Figure 4.9-maximum output of the photodiode in relation to distance between the two.

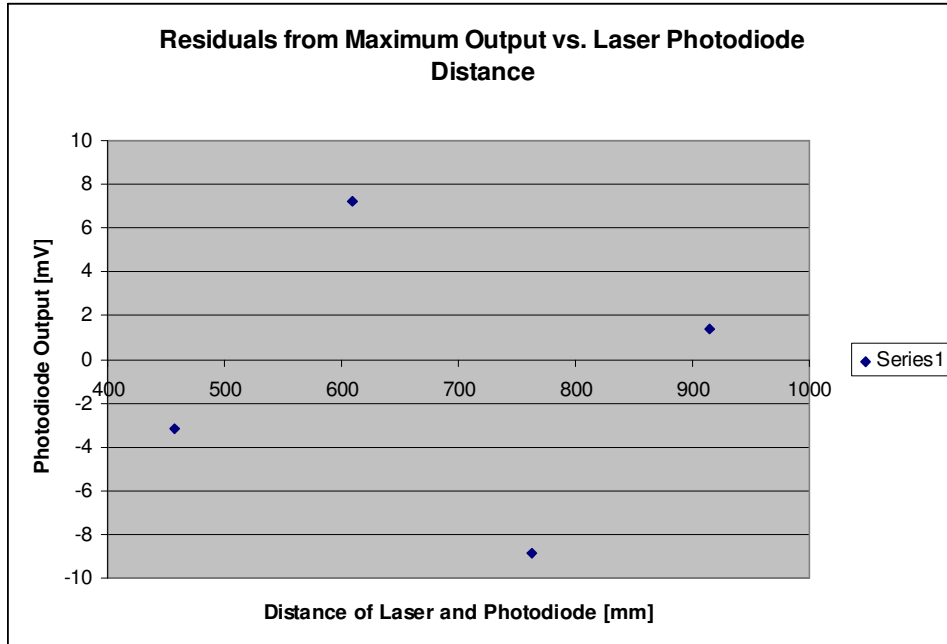


Figure 4.10-Shows the residuals from the first section of Figure 4.9.

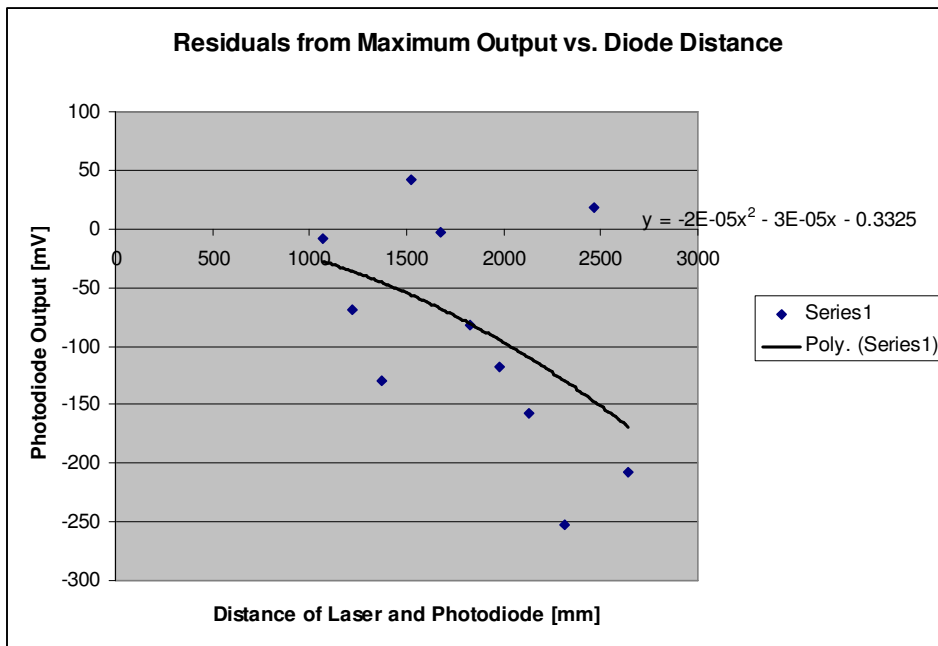


Figure 4.11-Shows the residuals of the second part of Figure 4.9.

The slope was then investigated for various placements of gauge blocks when the laser and photodiode are located 104 inches apart. Table 4.2 shows the resulting slopes and Figure 4.12 shows the residuals for the corresponding linear fits of the slopes. The difference in slopes varies with placement of the gauge block but not in any predictable way. Combined with the large residuals, this seems to indicate problems parallelizing the laser beam to the laser table. This is the one parameter besides block placement that changes every data run and is never perfect. With this in mind and no discernable pattern it seems evident that this is the culprit for the large residuals.

Distance of gauge block from laser Inch	Slope mV/ μ m
1	-1.44
26	-1.4
52	-1.45
103	-1.6

Table 4.2-Shows the slopes for various gauge block placements along the laser table when the laser and photodiode are 104 inches apart.

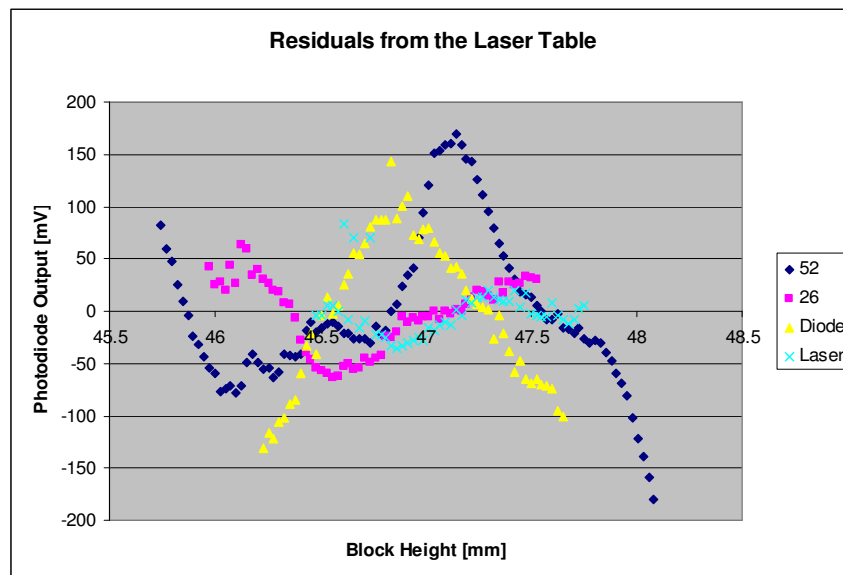


Figure 4.12-Shows the residuals from linear fits of data runs on the laser table with a distance of 104 inches between the laser and photodiode.

4.3 Conclusions

The laser beam's dispersion along with parallelizing the laser beam have been the biggest difficulties in developing this system. Figure 4.12 shows the residuals from the photodiode at a full distance and parallelized to the best of the lab's ability. It seems like the ideal utilization of the flatness scanner would be to measure the wire plane in increments of 36 inches or less. This way the beam will not have become so dispersed that it is wider than the photodiode and only the concerns with non uniformity of the laser or photodiode will need to be taken into account. Also, parallelizing the beam will become more manageable and the data will be more reproducible as shown in Figure 4.6.

Lastly, the laser and photodiode should be examined separately so as to find where the non uniformity rests. It would be recommended in any case to invest in another photodiode with a larger surface. Fitted with a filter to accept only light with a 670nm wavelength, the lights from the room should not have a heavy impact, and less concern will be needed in making the laser beam parallel.

Chapter 5

GARFIELD Simulations

5.1 Introduction to GARFIELD

The second half of the project has been the utilization of GARFIELD, a simulation program for drift chambers designed by Rob Veenhof, to examine sensitivity of electrons' drift time to imperfections in wire placement [1]. GARFIELD reads in information of the drift chamber, properties of the gas mixture, and track information of the electron that is created in an input file. From these input values GARFIELD is able to calculate the arrival time of avalanche electrons. The input files can be found in the appendix section of this thesis.

5.2 Garfield Simulations

GARFIELD constructs a wire chamber with the orientation depicted in Figure 5.1

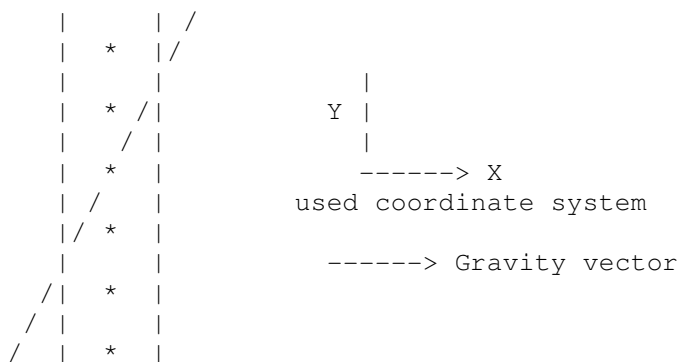
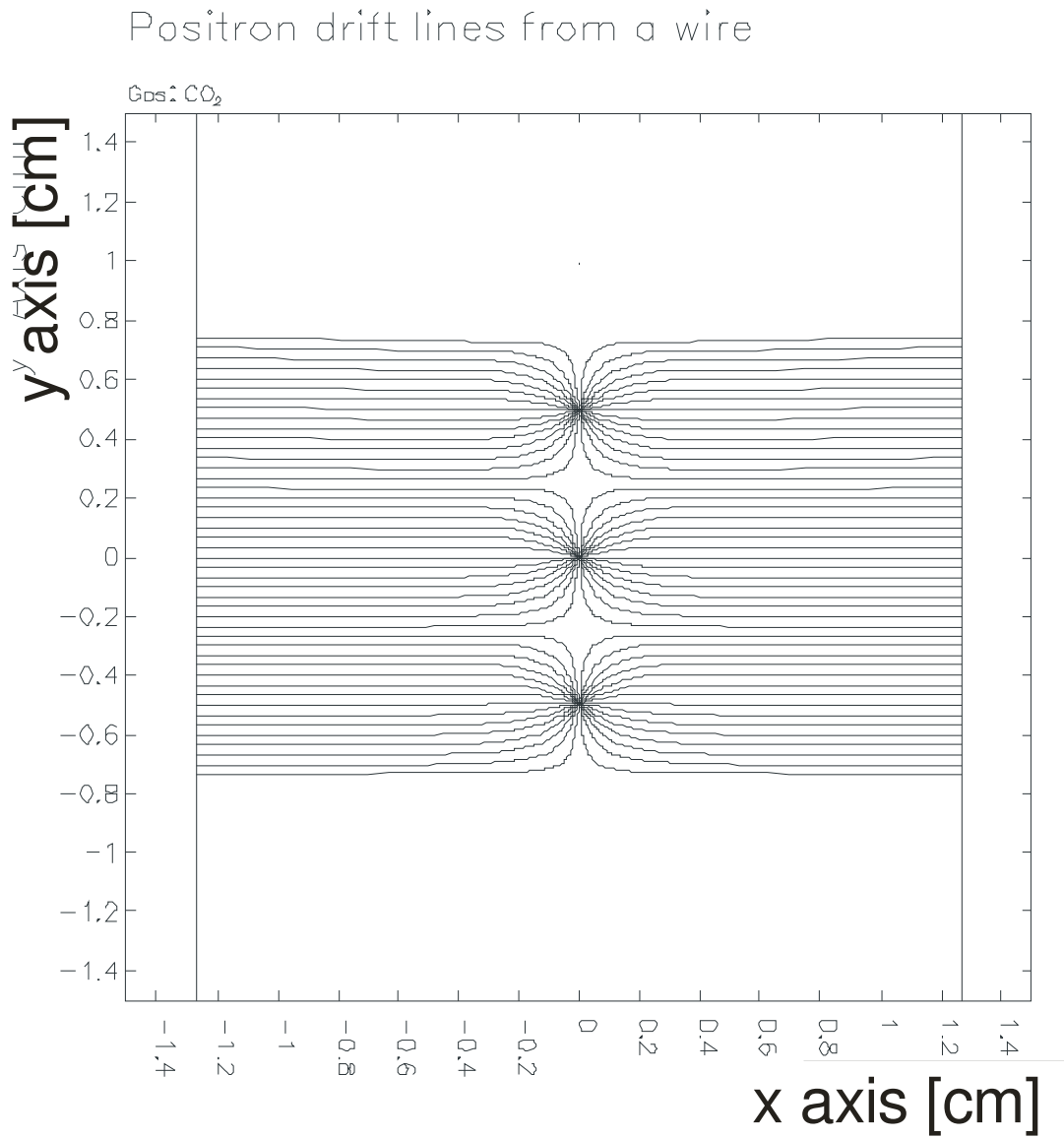


Figure 5.1-Shows the orientation used by GARFIELD for the simulations of the drift chambers. The angle is defined as the track and the x axis.

With this orientation and building on previous input files [reference] a new wire chamber composed of eleven perfectly placed wires was constructed in the cell.gar file. Figures 5.2 and 5.3 illustrate the electric field lines and equipotential lines of an ideal wire chamber. Utilizing this configuration the program was executed for electrons whose paths ranged for angles of 45° to 55° step 1° . The program also simulated an electron entering the wire chamber for multiple track offsets. From this data the drift times of the avalanche electrons were taken.



c

Figure 5.2-GARFIELD simulation of the electric field lines focusing on the center three wires in a wire chamber with perfect wire placement.

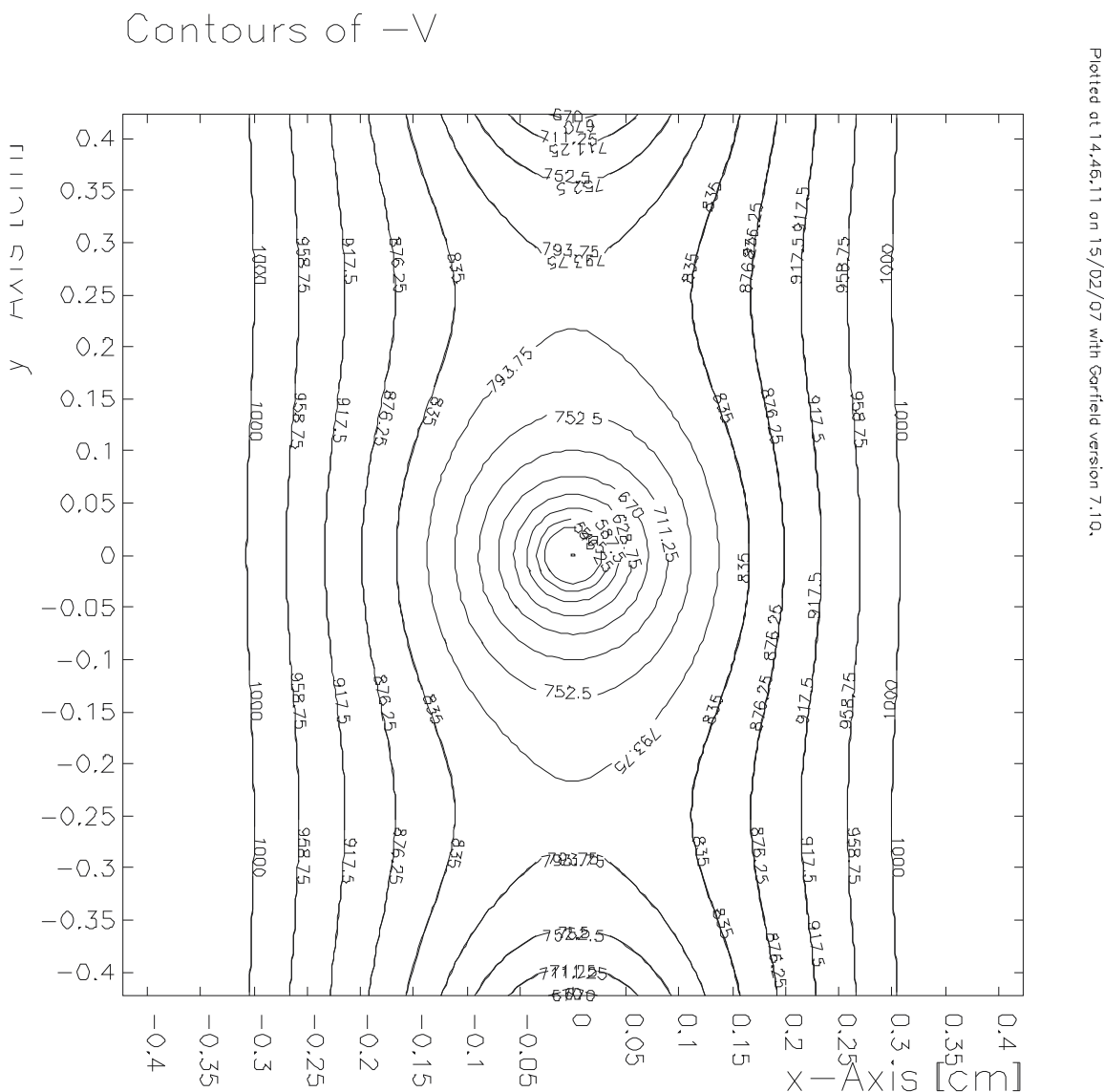
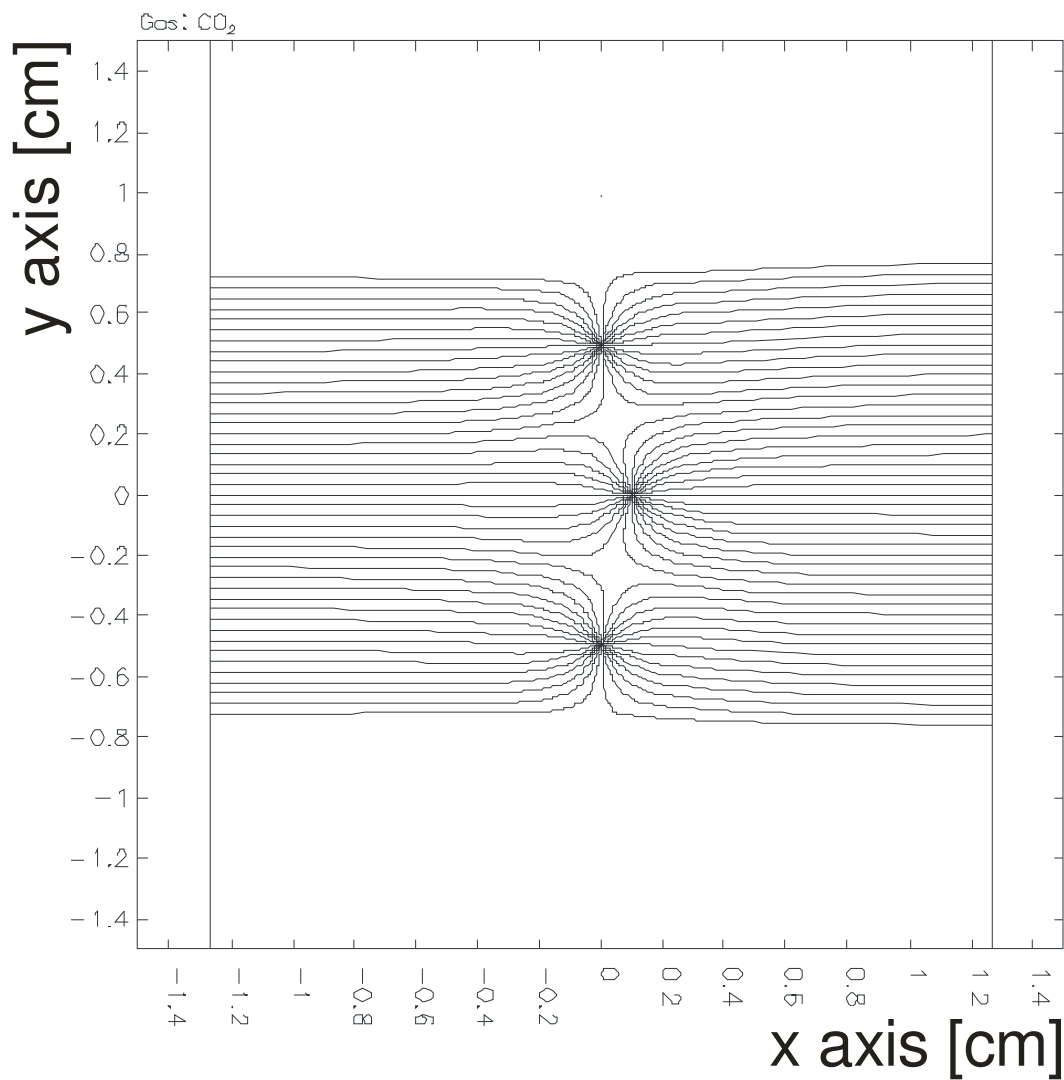


Figure 5.3-GARFIELD simulation of the equipotential voltage lines around the center wire of a wire chamber with perfect wire placement.

The wire was then systematically offset in the x direction. An initial step size of $25\mu\text{m}$ was used up to a distance of 0.025mm . From this point a step size of $50\mu\text{m}$ was used to increase the offset to 0.1mm . Figure 5.4 and 5.5 shows the electric field lines and voltage equipotential lines of a wire chamber that's center wire is offset by 0.1mm . The results of each of these were then compared to the results of a wire chamber with perfect

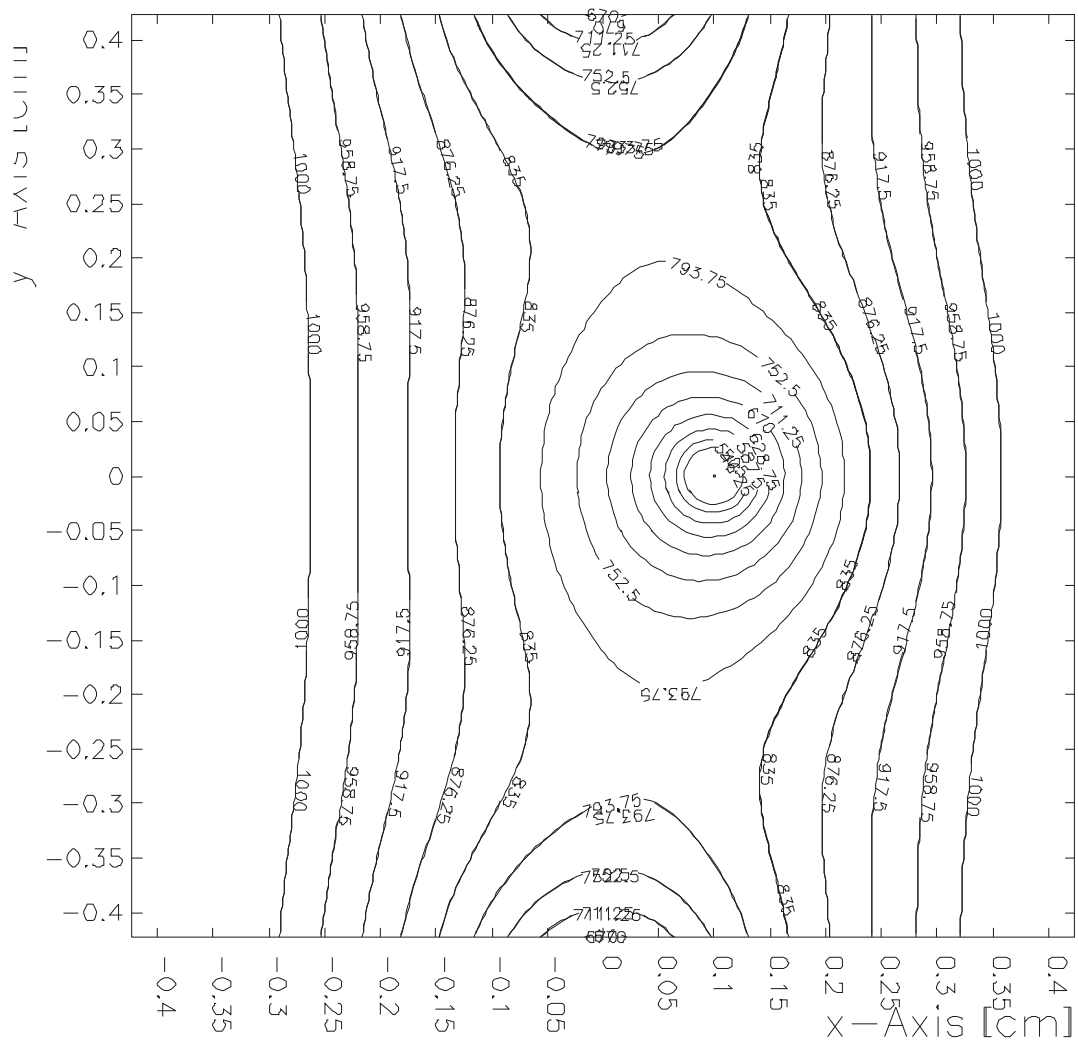
wire placement. Figures 5.4 and 5.5 demonstrate the effects of wire offset on the electric field and voltage equipotential lines.



Printed on 23/19/97 on 27/03/07 with garfield version 7.1.0.

Figure 5.4-GARFIELD simulation of the electric field lines focusing on the center three wires in a wire chamber with a center wire offset of 0.1mm.

Contours of $-V$



Plotted at 23:19:57 on 27/03/07 with Garfield version 7.10.

Figure 5.3-GARFIELD simulation of the equipotential voltage lines around the center wire of a wire chamber with a center wire offset of 0.1mm.

5.3 GARFIELD Results

The drift times for each wire offset were then compared to the drift time for a drift chamber with no offset. The nominal drift time was subtracted from the drift time for

each wire offset. This was then plotted for each angle. Below are the results for 45°, 50°, and 55°

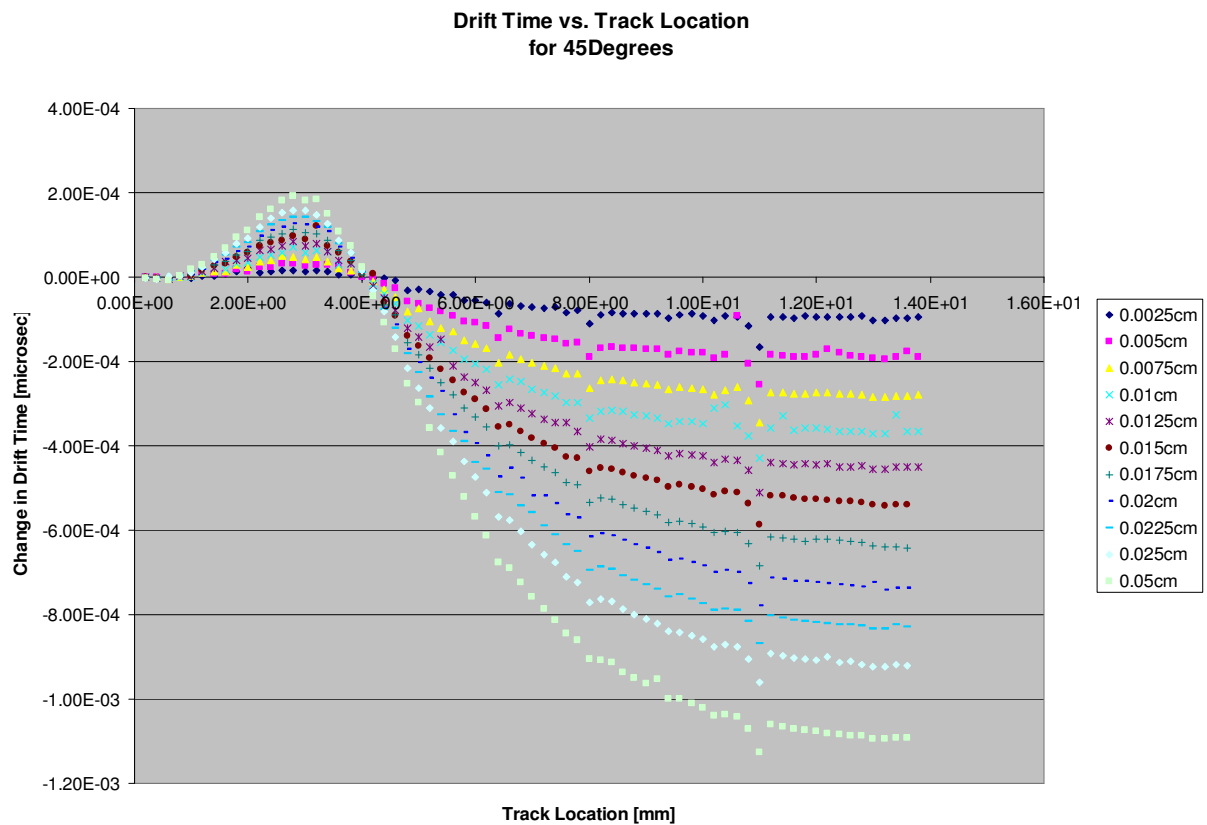


Figure 5.4-Depicts the change in drift time for 45° for wire offsets up to 0.025cm.

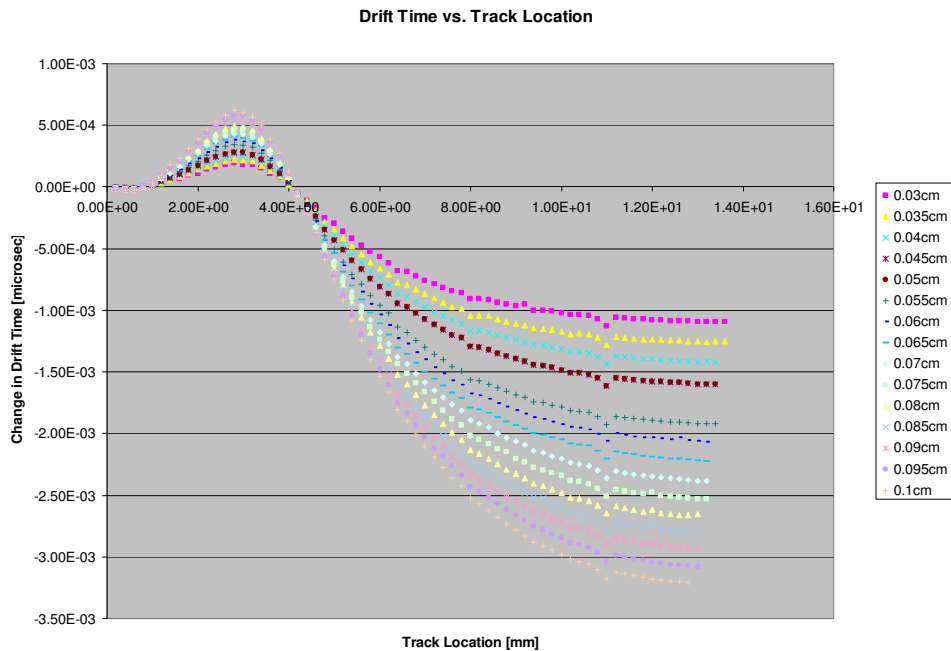


Figure 5.5-Depicts the change in drift time for 45° for wire offsets from 0.03cm to 0.1cm.

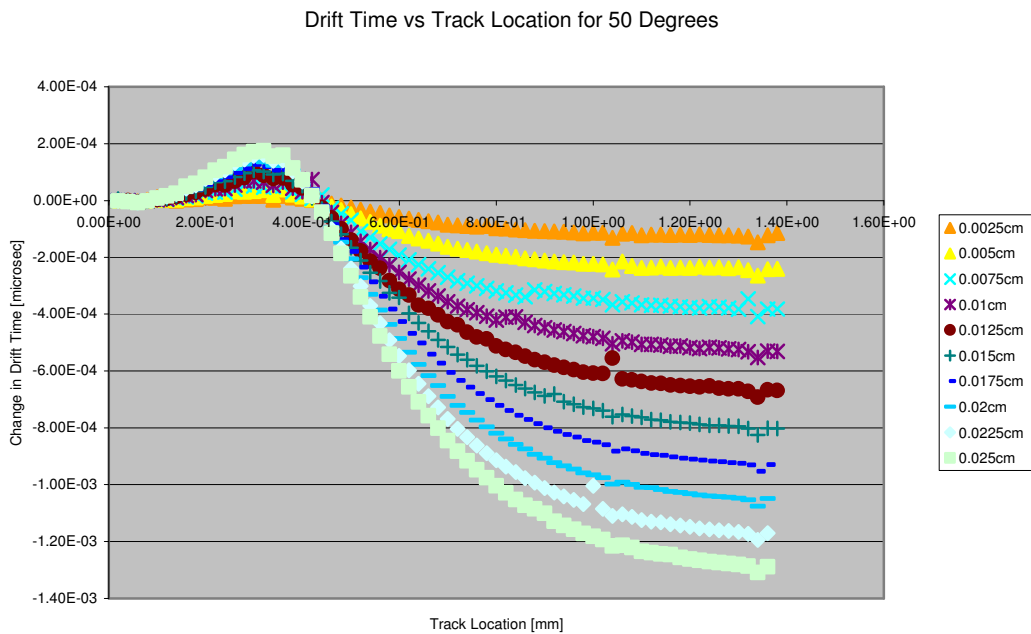


Figure 5.6-Depicts the change in drift time for 50° for wire offsets up to 0.025cm.

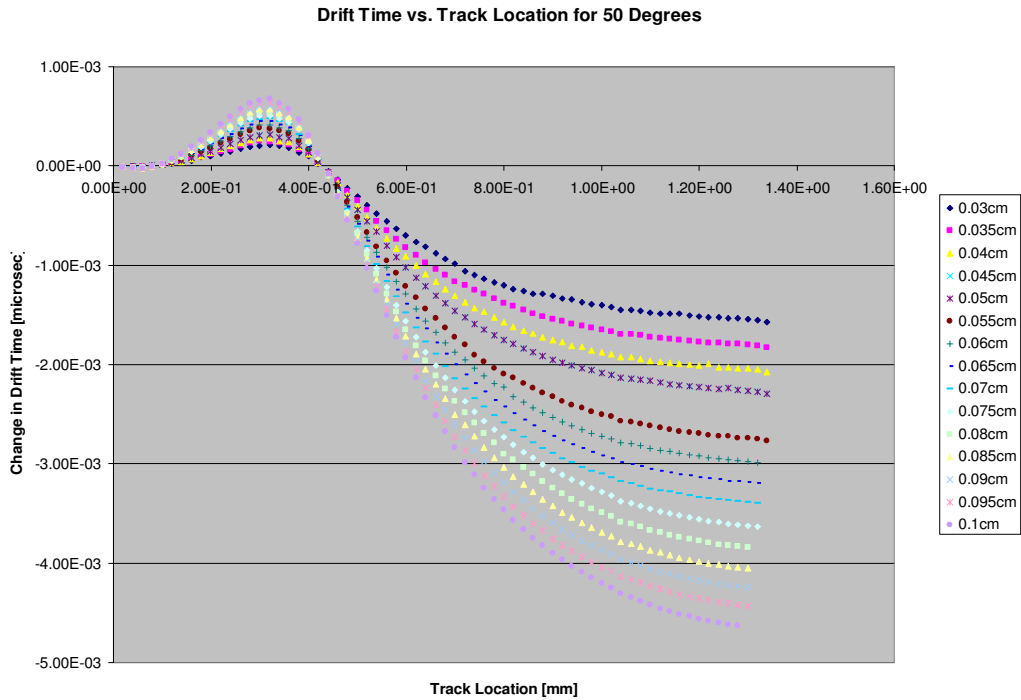


Figure 5.7-Depicts the change in drift time for 50° for wire offsets from 0.03cm to 0.1cm.

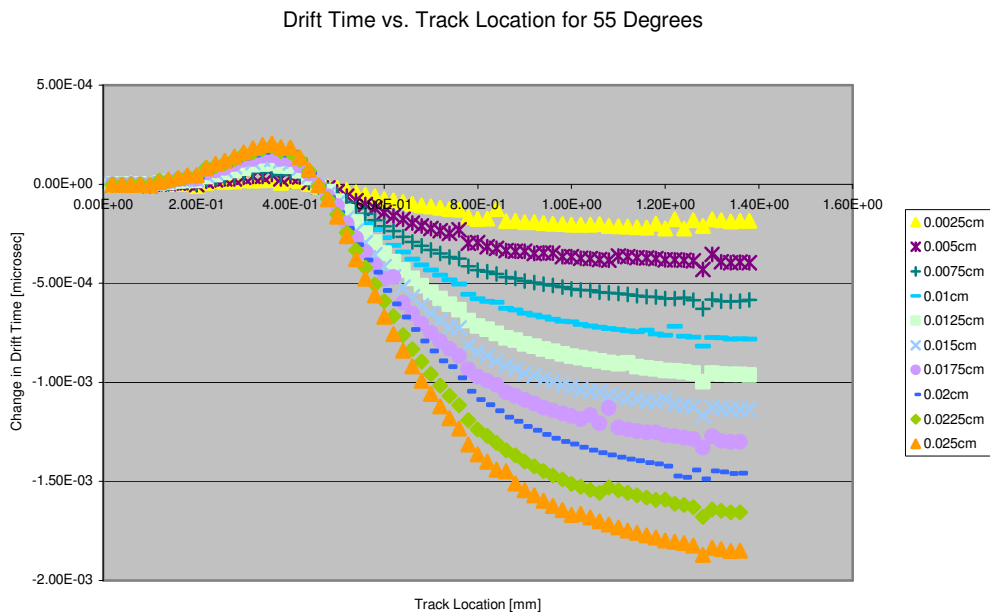


Figure 5.8-Depicts the change in drift time for 55° for wire offsets up to 0.025cm.

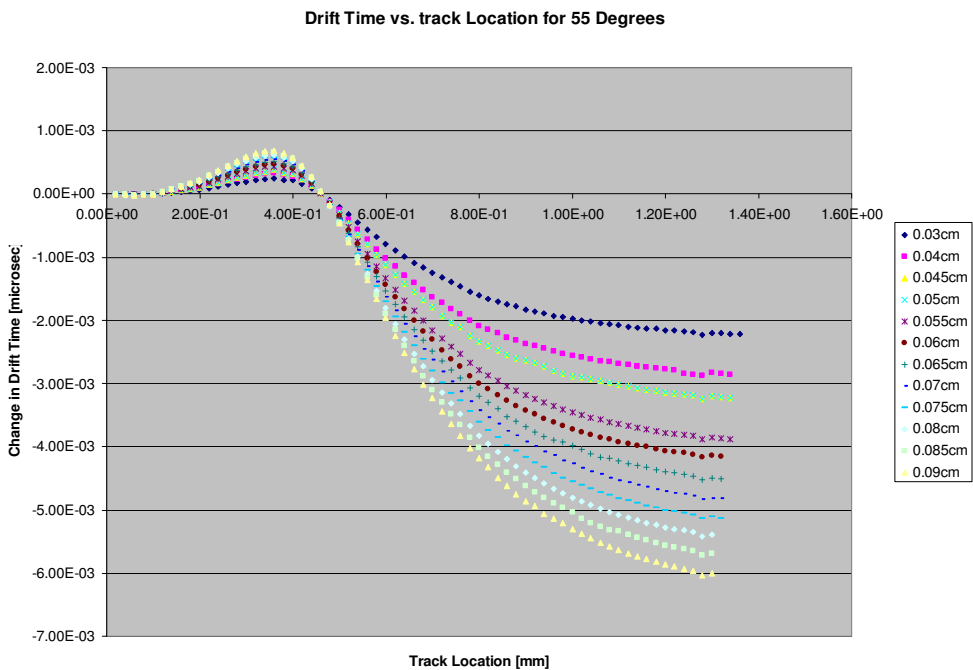


Figure 5.9-Depicts the change in drift time for 55° for wire offsets up to 0.1 cm.

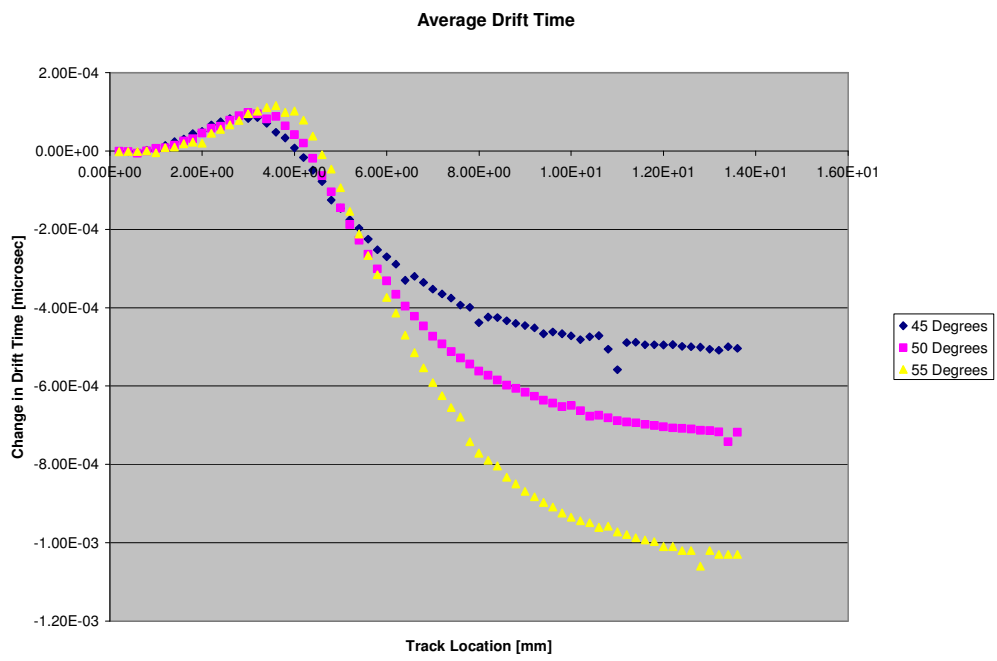


Figure 5.10- Average electron drift time for track location of 0.0025cm to 0.025cm.

5.4 GARFIELD Conclusions

The GARFIELD plots above give some very clear information about sensitivity to wire placement. Figures 5.11 5.12 give a better understanding of how the basic electric field lines change with wire offset. Figure 5.11 shows an ideal wire chamber with some electron tracks transversing the cell. Figure 5.12 shows the electric field lines for a wire chamber that has a center wire offset of 1 mm with the same set of tracks transversing the cell. It is evident that there will not be much of a drift time change for track offsets of less than about 2mm. This is because the electrons will be kicked out so close, and the electric field is so strong that the avalanche electrons quickly reach a high velocity. The next regions from approximately a 2mm to 4mm track offset will actually decrease the arrival time. This is due to the avalanche electrons capturing an electric field line that is more sharply angled in to the wire. Lastly, it is seen that drift time increases past the ~4mm mark. Here the change in drift time spread out into a spectrum. This is merely due to the avalanche electrons hitting the electric field at a point more distant to the wire and thus taking longer to arrive at the wire.

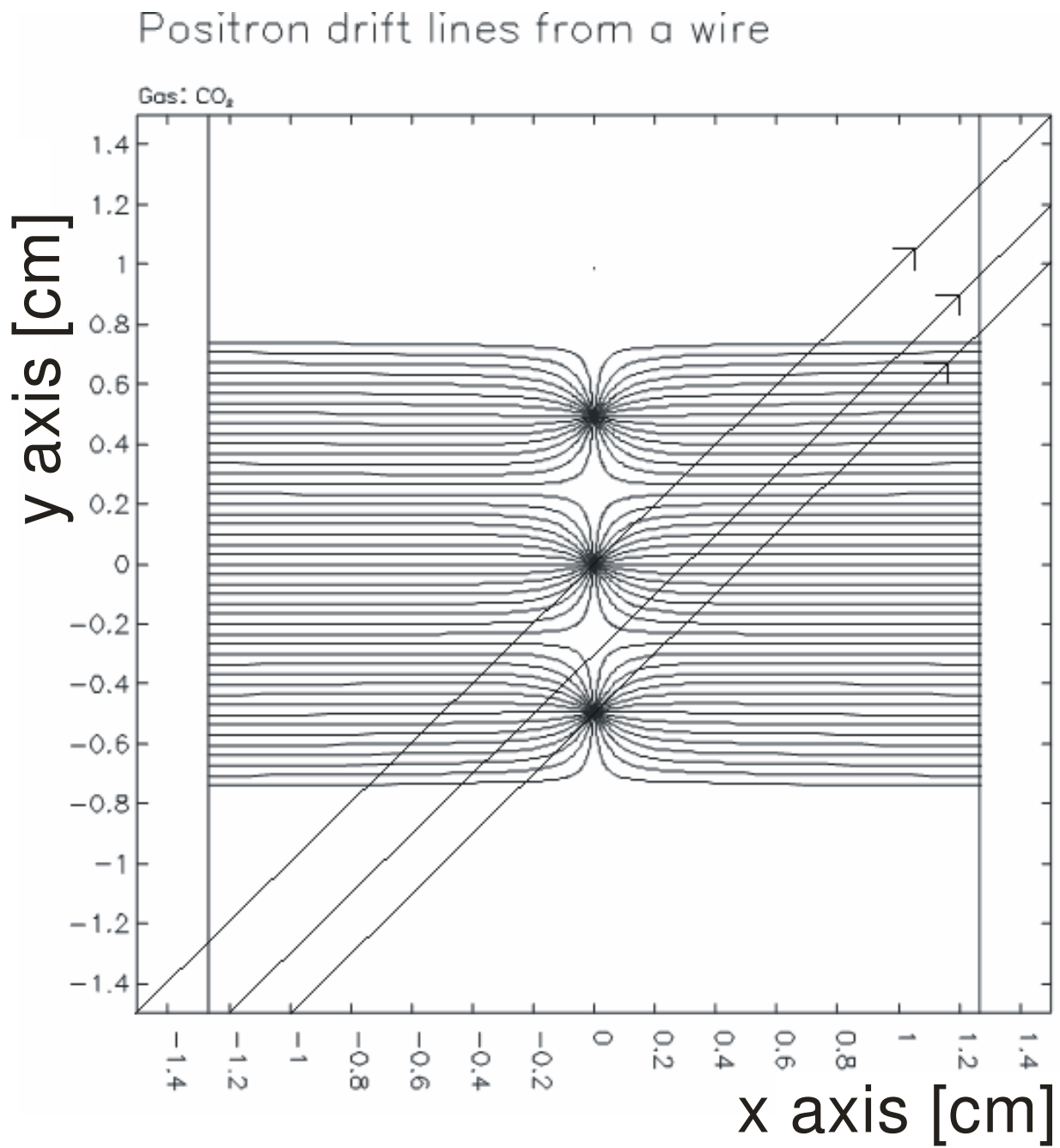


Figure 5.11-GARFIELD simulation of the electric field lines for a perfect wire chamber. Superimposed are three possible electron paths.

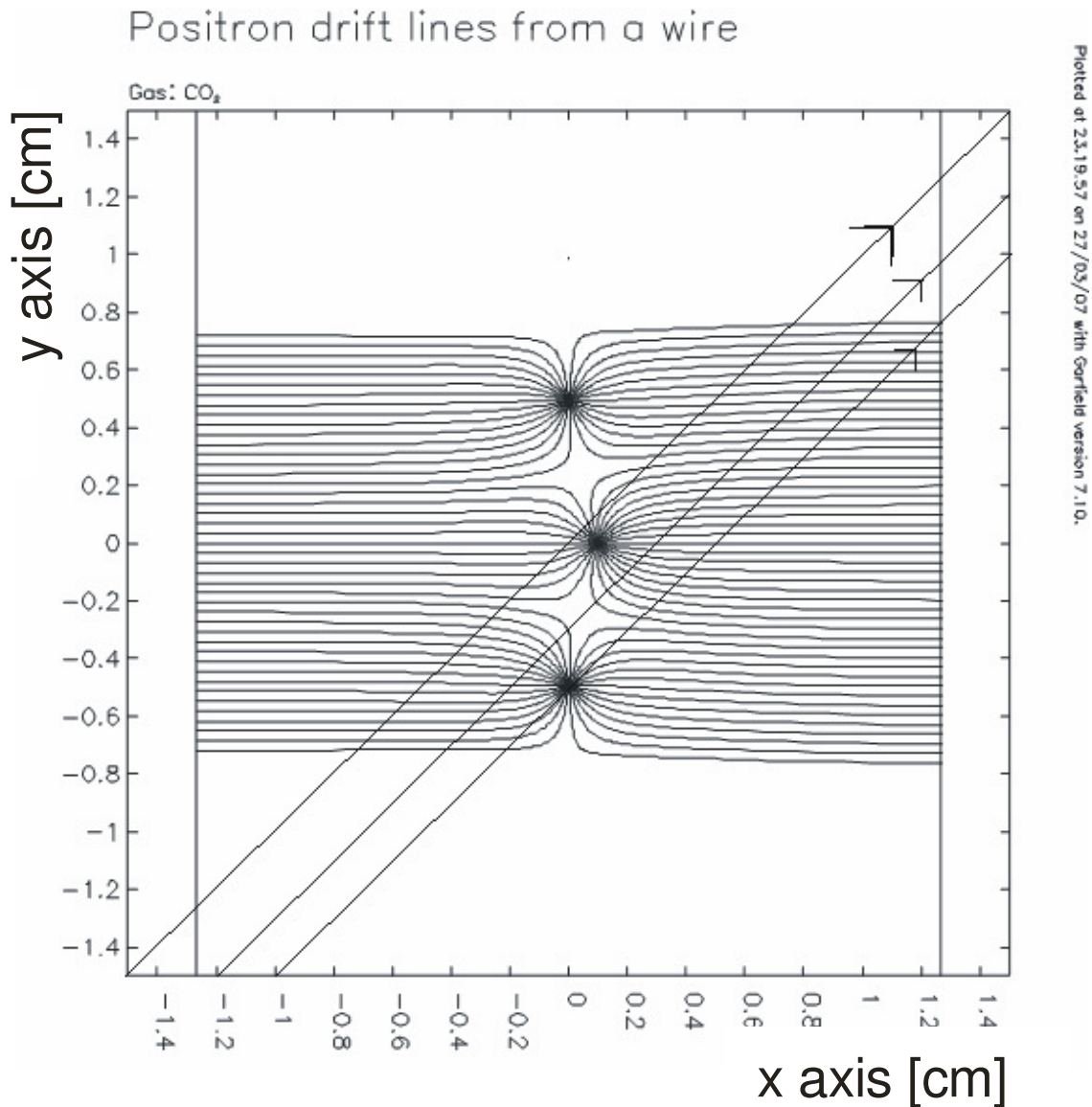


Figure 5.12-GARFIELD simulation of the electric field lines for a wire chamber that's center wire is offset by 1mm. Superimposed are three possible electron paths.

The two primary relationships that are observed are the dependency on primary electron entry angle and track location. Figure 5.10 gives a very clear indication of this. This graph averages the drift time for track locations of 0.0025mm to 0.025mm for 45°, 50°, and 55°. As can be seen the sensitivity to drift time change from wire placement increases with the entry angle. The other primary relationship is the sensitivity to track location, especially far from the wire. Both of these observations make sense because

given the wire offset in the positive x direction as well as the track location being in the positive x direction, the decrease in distance between the two will be exaggerated from the acceleration that the avalanche electrons experience. The sensitivity to the primary electron entry angle can be understood by looking at the limits. An entry angle of 0° would have almost no effect at all on the drift time whereas an entry angle of 90° would relegate the drift time to be correlated almost entirely to the track location.

Although the simulations were completed for wire offsets of up to 1mm it is unlikely that the actual wire offsets will be more than 0.5mm. With this in mind and looking at an entry angle of 55° there should only be a maximum change in drift time of about 2.3 ns. From the drift time calculations it appears that the longest time for a 55° with a electron track at touching the edge of the wire chamber is approximately 2 microseconds. This yields a average drift velocity of $60\mu\text{m}/\text{ns}$. So our absolute maximum error will be $138\mu\text{m}$, which is slightly above the goal of $100\mu\text{m}$ precision. However this all of the compounding errors will be unlikely to occur in the construction of the wire chamber, and should be able to be detected and repaired if they do appear.

The GARFIELD simulations were succesful, and showed that, with the errors that are expected with wire placement, the erros in driit distance will not be significant. However, modifications in the flatness scanner will need to be made to ensure that the wire ofests are within the acceptable errors based on the GARFIELD Simulations.

Appendix A. GARFIELD Input

The following input files for GARFIELD were created by Klaus Grimm [2]. They have been modified from their original configuration for the purpose of this thesis.

A.1 Cell

This input file describes the physical configuration of the wire chamber, including wire placement, position of the high voltage planes, and the charges of each.

```
//=====
// Garfield V8.1 Input file for:
//
// Vertical Drift Chamber (VDC) Simulation
// for the Qweak experiment at JLab
//
// => generates the CELL definition
// file needed for additional Garfield
// simulations:
// FIELD, XT, ARRIVAL-TIME-DISTRIBUTION,
// TIMING, SIGNAL
//
//=====
// Simplified VDC layout for Garfield
//
// VDC consists of one wire plane and two HV planes.
// Garfield forces us to use this orientation of the VDC since
// in Garfield you can only define a X-RANGE **only** for a XT-PLOT
...
// (There is no YT-PLOT or Y-RANGE for XT-PLOT defined in Garfield)
//
//      |      | /
//      | *  | /
//      | * /|      |
//      | / |      Y |
//      | * |      |
//      | / |      -----> X
//      | / |      used coordinate system
//      | / * |
//      |   |      -----> Gravity vector
//      /| * |
//      / | | |
//      / | * |
//
//=====
//
// Author: Klaus Grimm
```

```

//          Department of Physics
//          The College of William and Mary
//          Williamsburg, VA 23185
//
// email: grimm@jlab.org
//
//=====
// Last Change: 07/18/2007
//=====
//
// Garfield units: cm ,V

GLOBAL anode      = -2000           // high voltage on
planes [V]

GLOBAL wnum       = 11              // Number of wires
GLOBAL plane      = 1.27            // distance wire
plane to HV plane (13mm)
GLOBAL pitch      = 0.494           // perp. distance
between signal wires (@26.57deg)

GLOBAL fheight    = 50.0            // inner frame height
GLOBAL gammaDEG   = 26.565         // wire stringing
angle to long VDC axis (deg)
GLOBAL gammaRAD   = pi/180.*gammaDEG // same in RAD

GLOBAL wdiameter  = 0.0025         // 25um wire diameter
GLOBAL wpot       = 0.0            // voltage on signal
wire = 0.0 V
GLOBAL wtension   = 70.0           // wire tention = 70g
GLOBAL wlength    = fheight/sin(gammaRAD) // overall wire length
(45deg)
//GLOBAL wlength   = 1000           // overall wire
length (45deg)

GLOBAL wxpos      = 0.0            // all signal wires
with x=0

GLOBAL xoffset    = 0.0            // offset of center
wire (#6) in cm

// Delete some result files, otherwise results from different
settings/simulations
// will be saved in the same file ...

//=====
& CELL
//=====

//-----
--
// Simplified VDC layout for Garfield
//

```

```

// Garfield forces us to use this orientation of the VDC since
// in Garfiled you can only define a X-RANGE **only** for a XT-PLOT
...
//
// | | |
// | * | Y |
// | | |
// | * | -----> X
// | | | used coordinate system
// | * |
// | | | -----> Gravity vector
//
//-----
----
opt cell-pr

// Location of the HV planes
plane x={-plane} v={anode}
plane x={+plane} v={anode}

//ROWS CARTESIAN
//S * {wdiameter} 0.05 -2.47 {wpot} {wtension} {wlength} Tungsten
//S * {wdiameter} {wxpos} 0.494 {wpot} {wtension} {wlength}
Tungsten

// Location of the signal wires
ROWS CARTESIAN
S * {wdiameter} {wxpos} -2.47 {wpot} {wtension} {wlength}
Tungsten
S * {wdiameter} {wxpos} -1.976 {wpot} {wtension} {wlength}
Tungsten
S * {wdiameter} {wxpos} -1.482 {wpot} {wtension} {wlength}
Tungsten
S * {wdiameter} {wxpos} -0.988 {wpot} {wtension} {wlength}
Tungsten
S * {wdiameter} {wxpos} -0.494 {wpot} {wtension} {wlength}
Tungsten
S * {wdiameter} {xoffset} 0.0 {wpot} {wtension} {wlength}
Tungsten
S * {wdiameter} {wxpos} .494 {wpot} {wtension} {wlength}
Tungsten
S * {wdiameter} {wxpos} .988 {wpot} {wtension} {wlength}
Tungsten
S * {wdiameter} {wxpos} 1.482 {wpot} {wtension} {wlength}
Tungsten
S * {wdiameter} {wxpos} 1.976 {wpot} {wtension} {wlength}
Tungsten
S * {wdiameter} {wxpos} 2.47 {wpot} {wtension} {wlength}
Tungsten

// Gravity points perp. to HV plane = x directection
GRAVITY 1 0 0

```

```
// Save this &CELL definition
WRITE DATASET vdc_cell_11.dat

//=====
& OPTIMISE
//=====

//Prints the current potential settings
DISPLAY

//forces acting on a wire and the wire displacement
SELECT 1
FORCES PRINT-SAG PLOT-SAG KEEP-SAG DETAILED ...
ELECTROSTATICS GRAVITY ...
SCANNING-GRID 25 25 ...
SCAN-AREA -0.15 -0.15 +0.15 +0.15

//=====
& QUIT
//=====
```

A.2 Field

The Field input files plots the electric field lines, contour plots, and vector fields of the electric field.

```
//=====
// Garfield V8.1 Input file for:
//
// Vertical Drift Chamber (VDC) Simulation
// for the Qweak experiment at JLab
//
//=====
// Realization in Garfield:
//
// VDC consists of one wire plane and
// two HV planes
//
//=====
//
// Author: Klaus Grimm
//         Department of Physics
//         The College of William and Mary
//         Williamsburg, VA 23185
//
// email: grimm@jlab.org
//
//=====
// Last Change: 04/02/2004
//=====

GLOBAL anode      = -4100          // high voltage on planes
GLOBAL wnum       = 41             // Number of wires
GLOBAL pitch      = 0.423          // perp. distance between signal
wires    (4.23mm)

GLOBAL wdiameter  = 0.002          // 20um wire diameter
GLOBAL wpot       = 0.0            // voltage on signal wire = 0.0 V
GLOBAL wtension   = 70.0           // wire tension = 70g
GLOBAL wlength    = 25.0*1.141     // overall wire length (45deg)

GLOBAL apitch     = 0.423*0.5      // half top    pitch size used for
ARRIVAL-TIME-DISTRIBUTION
GLOBAL tpitch     = apitch*1.41    // bit more than bottom half pitch
size used for TIMING

GLOBAL plane      = 1.27           // distance wire plane to HV plane
(13mm)
GLOBAL wxpos      = 0.0            // all signal wires with x=0
GLOBAL wstart     = -20*pitch      // position of first signal wire:
y=-8.46mm
```

```

// Specify the gas-file to be loaded
Global gas_file      `Ar-C2H6_50-50.gas`
//Global gas_file    `Ar-C2H6_63-37.gas`
//Global gas_file    `Ar-CO2_90-10.gas

//=====
& CELL
//=====

// Load &CELL definitionwxpos
GET vdc_cell_11.dat

//=====
& MAGNETIC
//=====

// at present: no B field here
// whats about the earth B field ?!
COMPONENTS 0 0 0 GAUSS

//=====
& GAS
//=====

// 1 atm 50/50 Argon-ethane mixture in your chamber.

// Load gas_file, which contains all
// the gas properties needed for tracking

Call inquire_member(gas_file,gas_member,`gas`,exist)

If exist Then
  get {gas_file}
Else
  Say "Gas file doesn't exist, please check"
Endif

// Plot some gas properties
// plot-options drift-velocity nodiffusion notownsend

opt gas-plot nogas-print

//=====
& OPTIMISE
//=====

//Prints the current potential settings
DISPLAY

//forces acting on a wire and the wire displacement
SELECT 6
FORCES PRINT-SAG PLOT-SAG KEEP-SAG DETAILED ...
ELECTROSTATICS GRAVITY

```

```

//-----
// Open Postscript file
//-----
!add meta type PostScript file-name "field.ps"
!open meta
!act meta

//=====
& FIELD
//=====

AREA {-1.1*plane, -2*pitch, +1.1*plane, +2*pitch}

// Plot electrical field
track -1.3 0.0 -0.01 0.0
PLOT-FIELD GRAPH sqrt(EX**2+EY**2)

//track * * -0.3 *
//PLOT-FIELD GRAPH sqrt(EX**2+EY**2)

//track -0.3 * -0.05 *
//PLOT-FIELD GRAPH sqrt(EX**2+EY**2)

//track -0.05 * -0.0001 *
//PLOT-FIELD GRAPH sqrt(EX**2+EY**2)

// Plot contour of Electrostatic potential
grid 25
area * -.423 * .423
PLOT-FIELD CONTOUR -V RANGE 10 2100 n=40

area -.423 * .423 *
PLOT-FIELD CONTOUR -V RANGE 10 1000 n=24

//=====
& DRIFT
//=====

//Sets the size and view of the drift area
AREA -1.5 -1.5 +1.5 +1.5

//Number of drift lines used by x(t) etc.
LINES 60

//Grid density for tables and contour plots
GRID 10 20

// define area around wire #21 for possible plots
SELECT 5 6 7 // select center wire

INTEGRATION-PARAMETERS COMPUTE-IF-INTERPOLATION-FAILS

```

```
// define single track: 45deg
TRACK -1.5 -1.5 1.5 1.5

// Heed takes care of cluster generation, it simulates the ionisation
of
// the gas molecules by a particle.
TRACK HEED ...
  NODELTA-ELECTRONS NOTRACE-DELTA-ELECTRONS ...
  NOMULTIPLE-SCATTERING ...
  NOENERGY-CUT ELECTRON ENERGY 1.165 GeV

// drift line calculation:
// will begin at some of the boundaries of the drift area as set by
AREA.
//DRIFT EDGE notleft notright up down isochrone 0.020

// drift line calculation:
// electrons or ions start to drift from the surfaces of the wires
that
// have been SELECTed.
// DRIFT WIRE lines 30 isochrone 0.020
DRIFT WIRE lines 30

// drift line calculation: will begin on the track.
//DRIFT TRACK TIME-GRAPH CONTOUR 0.020

//-----
// Close Postscript file
//-----
!deact meta
!close meta
!del meta
```

A.3 XT

The following input file generates tables of drift times.

```
//=====
// Garfield V8.1 Input file for:
//
// Vertical Drift Chamber (VDC) Simulation
// for the Qweak experiment at JLab
//
// => Simulation of the XT-Plot
//   Correlation between perp. track distance to the wire plane and
//   the drift time of the first electron hitting the selected wire
//
//=====
//
// Simplified VDC layout for Garfield
//
// VDC consists of one wire plane and two HV planes.
// Garfield forces us to use this orientation of the VDC since
// in Garfield you can only define a X-RANGE **only** for a XT-PLOT
...
// (There is no YT-PLOT or Y-RANGE for XT-PLOT defined in Garfield)
//
//   |   | /
//   | *  | /
//   |   |   |
//   | * /|   | Y |
//   | / |   |   |
//   | * |   |   | -----> X
//   | / |   |   | used coordinate system
//   | / * |   |
//   |   |   |   | -----> Gravity vector
//   /| * |
//   / | * |
//   / | * |
//
//=====

// Author: Klaus Grimm
//         Department of Physics
//         The College of William and Mary
//         Williamsburg, VA 23185
//
// email: grimm@jlab.org
//
//=====
// Last Change: 05/25/2005 - BY CARISSA
// Altered angle range: Now [40,60]
//=====

GLOBAL tanglemin = 45.0
GLOBAL tanglemax = 55.0
```

```

GLOBAL tanglestep = 1.0

GLOBAL plane      = 1.27          // distance wire plane to HV plane
(13mm)
GLOBAL pitch      = 0.494        // perp. distance between signal
wires (7/16"@26.565deg)
GLOBAL apitch     = pitch*0.5    // half top pitch size used for
ARRIVAL-TIME-DISTRIBUTION
GLOBAL tpitch     = apitch*1.41  // bit more than bottom half pitch
size used for TIMING

GLOBAL xstep      = 0.05         // Coarse stepping size in X for
tracks (0.05=50um)
GLOBAL xfstep     = 0.02         // Fine stepping size in X for
tracks (0.02=200um)

// Specify the gas-file to be loaded
Global gas_file   `Ar-C2H6_50-50.gas`
//Global gas_file `Ar-C2H6_63-37.gas`
//Global gas_file `Ar-CO2_90-10.gas`

//=====
& CELL
//=====

// Read &CELL definition
GET vdc_cell_11.dat

// Gravity points perp. to HV plane = x directection
GRAVITY 1 0 0

//=====
& MAGNETIC
//=====

// at present: no B field here
// whats about the earth B field ?!
COMPONENTS 0 0 0 GAUSS

//=====
& GAS
//=====

// Load existing gas_file, which contains all
// the gas properties needed for tracking

Call inquire_file(gas_file,exist)

If exist Then
  get {gas_file}
Else
  Say "Gas file doesn't exist, please check"
Endif

//=====
& DRIFT

```

```

//=====

INTEGRATION-PARAMETERS COMPUTE-IF-INTERPOLATION-FAILS

// Heed takes care of cluster generation, it simulates the ionisation
of
// the gas molecules by a particle.
TRACK HEED ...
  NODELTA-ELECTRONS NOTRACE-DELTA-ELECTRONS ...
  NOMULTIPLE-SCATTERING ...
  NOENERGY-CUT ELECTRON ENERGY 1.165 GeV

//Sets the size and view of the drift area
AREA {-1.1*plane, -1.0*tpitch, +1.1*plane, +1.0*tpitch}

//Number of drift lines used by x(t) etc.
LINES 100

// define area around wire #6 for possible plots
SELECT 6 // select center wire

//-----
// Open Postscript file
//-----
!add meta type PostScript file-name "xt.ps"
!open meta
!act meta

GLOBAL count = 0 // count is used to name the output files

FOR tangle from {tanglemin} to {tanglemax} STEP {tanglestep} DO

// delete old entries from previous simulations
* %DELETE "XT_{angle}deg_S21.dat" .

// XT-PLOT: relation between the perp. position of a track and the
drift time.
// This is a calibration curve used by the track reconstruction program

Say "Simulating now XT-PLOT for incident angle = {tangle}"

  XT-PLOT ...
  ANGLE {tangle} ...
  X-RANGE {xfstep , 1.1*plane} X-STEP {xfstep} ...
  PRECISION 1E-4 ...
  PLOT-XT-RELATION ...
  DATASET "{count}_XT_S6.dat" // tangle replaced with count in
filename

GLOBAL count = count + 1 // increment counter

ENDDO

//-----
// Close Postscript file
//-----

```

```
!deact meta  
!close meta  
!del meta
```

References

- [1] Veenhof, Rob. “Simulation of Gaseous Detectors”. Abstract.
<http://consult.cern.ch/writeup/GARFIELD/>. Version 7.04. 25 Jan 2001.
- [2] Compilation and source help by Klaus Grimm
http://www.jlab.org/~grimm/Qweak/GARFIELD/GARFIELD_Sources.html
- [4] Armstrong et al. “The Qweak Experiment: A Search for New Physics at the TeV Scale
Via the Measurement of the Proton’s Weak Charge.”
“<http://www.jlab.org/qweak/>” (2001).
- [5] Sauli, F. *Principles of Multiwire Proportional and Drift Chambers*. European Organization for Nuclear Research [CERN]. Lecture. Geneva 1977.
- [6] PowerPoint presentation on VDCs by Dr. Klaus Grimm in Boston
<http://www.jlab.org/~grimm/Qweak/talks/Boston/>
- [7] Epperson, Erin H. *Software and Simulation for Q_{weak}* [thesis]. Williamsburg (VA): College of William and Mary; 2004 April.
- [8] PowerPoint presentation on VDCs by Dr. Klaus Grimm in Boston
<http://www.jlab.org/~grimm/Qweak/talks/Boston/>